◀ **Fig. 2** Photomicrographs of immunohistochemical staining for phosphorylated α-synuclein in paraffin sections of bodily organs and tissue. Positive staining is *black*, the counterstain is neutral red. **a**, **b** Low and higher magnification images of the submandibular gland in two subjects with PD, showing immunoreactive nerve fibers within the stroma of the gland. *Calibration bar* in **a** 0.2 mm; in **b** 100 μm. **c** The submucosa of the lower esophagus of a subject with PD, showing immunoreactive puncta, fibers and perikaryal cytoplasmic inclusions in ganglion cells. **d** Immunostaining of fibers in the duodenal submucosa of a subjects with DLB. *Calibration bar* 20 μm. **e** A single immunoreactive fiber in the stroma of the pancreas from a subject with PD. *Calibration bar* 40 μm. **f** A single immunoreactive fiber in the submucosa of a primary bronchus of a subject with PD. *Calibration bar* 40 μm. **g** A few immunoreactive fibers in the submucosa of the larynx of a subject with PD. *Calibration bar* 20 μm. **h** Several immunoreactive fibers in an epicardial nerve twig entering the myocardium in a subject with DLB. *Calibration bar* 100 μm. **i** A single immunoreactive fiber in the intermyenteric plexus of the urinary bladder of a subject with DLB. *Calibration bar* 20 μm. **j** Frequent immunoreactive fibers, puncta as well as cells with diffusely stained perikaryal cytoplasm in the adrenal medulla of a subject with PD. *Calibration bar* 100 μm. **k** A single immunoreactive fiber in the stroma of the parathyroid gland of a subject with PD. *Calibration bar* 10 μm. **l** The ovary of a woman with PD showing diffuse perikaryal immunostaining of a neuron-like cell with adjacent immunoreactive fibers and puncta. *Calibration bar* 10 μm

Subjects with ILBD and ADLB had much lower frequencies of positive staining in body regions (Fig. 4a, d). In subjects with ADLB, positive staining was limited entirely to the spinal cord and sympathetic ganglia, with only 1/18 and 2/18 subjects affected, respectively. Subjects with ILBD showed higher frequencies of positive staining than ADLB subjects in the spinal cord, sympathetic ganglia, vagus nerve and gastrointestinal tract while all other areas, as with the ADLB cases, showed no positive staining. When several microscopic slides from each spinal cord subdivision were stained, 5/6 of the ILBD cases had PASH present while on single-slide analysis, only 1 of 6 subjects had been positive. For the ADLB subjects for which serial paraffin and 80-μm sections of submandibular gland and esophagus were examined, 3/15 were found to be positive, whereas examination of single paraffin sections had found no positively stained structures. Figure 4e depicts the regional staining distribution, derived from analysis of a single slide per region, when data from all subjects were combined. This shows generally the same pattern as for PD and DLB subjects.

Table 6 and Fig. 5a and b show the regional distribution and density of PASH within paraffin sections on single slides of the major subdivisions of the spinal cord as well as cervical and thoracic sympathetic ganglia, for all subjects combined. The frequency of positive staining between different cord regions is similar, with the cervical cord being the least-often affected (Fig. 5a). In terms of the density scores, the thoracic and sacral cord regions have higher mean scores than the cervical and lumbar regions. Cervical sympathetic ganglia had the highest frequency and mean density scores of any region.

Table 7 and Fig. 5c and d show the regional distribution and density of PASH within major sites within the gastrointestinal (GI) system. There is a marked trend for a diminishing rostrocaudal gradient. The submandibular gland and lower esophagus have the highest frequency of PASH, followed by the stomach, small bowel regions, large bowel regions and rectum. The data shown for submandibular gland and esophagus do not include, to provide an unbiased comparison between GI regions, results from the serial paraffin or 80-μm sections. As mentioned previously, when staining from these extra sections was considered, a higher percentage of subjects were graded as positive. A striking finding was the complete absence of positive staining in upper esophagus and therefore all data for esophagus shown are derived from analysis of the lower esophagus. Although not quantitatively assessed here, it was apparent that PASH was more frequently present in the myenteric plexus than in the submucosal plexus.

Discussion

The results of this investigation support prior studies [12, 14, 17–19, 29, 40, 48, 81] that have indicated that PASH is widespread throughout the spinal cord and peripheral nervous system of subjects with PD. The present study adds to this body of knowledge by providing data for other Lewy body disorders including DLB, ILBD and ADLB, by surveying many more sites than had previously been investigated, and using large enough sample sizes to provide preliminary estimates of the relative frequency and density of α-synuclein histopathology at these locations. In addition, the use of a method that is specific and sensitive for phosphorylated α-synuclein, which is detected only in pathological structures [34] effectively eliminates the ambiguity of staining results derived using antibodies that recognize normal α-synuclein.

For spinal cord and sympathetic ganglia, subjects with PD as well as DLB invariably have PASH in the regions of the cord containing preganglionic autonomic neurons as well as within sympathetic ganglia. Because these neurons project widely throughout the body, it is highly probable that, for subjects with PD and DLB, that α-synuclein histopathology is also very widely present within the end-organ targets of the autonomic nervous system, although a full test of this hypothesis will require multiple-section examination of each of the many sites [49]. This study has found that the relative frequency of PASH in end-organs was generally much lower than in the spinal cord or sympathetic ganglia, but when sampling was expanded

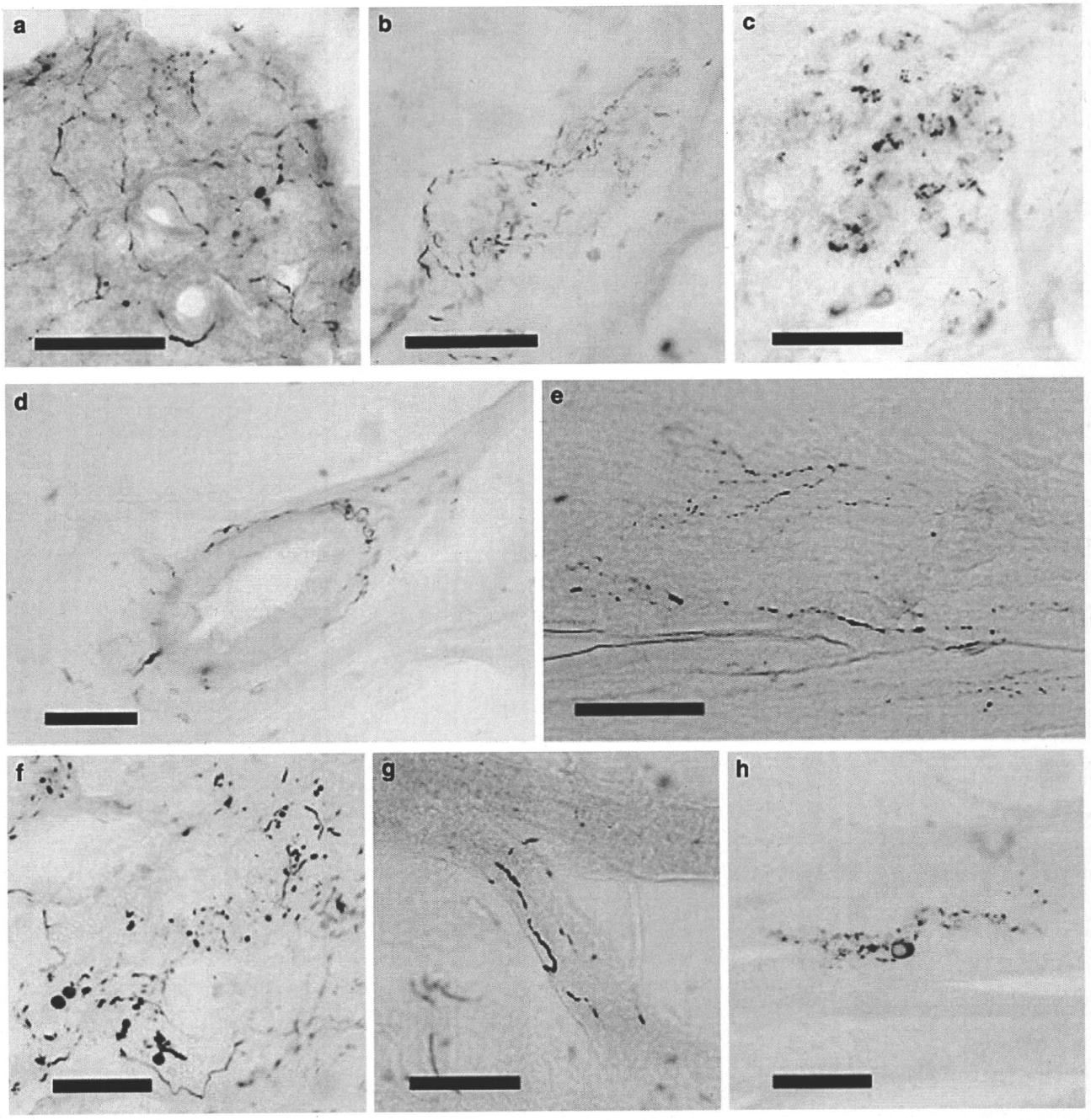

Fig. 3 Photomicrographs of immunohistochemical staining for phosphorylated α-synuclein in 80-μm thick frozen sections of formalin-fixed, cryoprotected tissue blocks of submandibular gland and lower esophagus. Positive staining is *black*. There is no counterstain. Submandibular gland from subjects with DLB (**a–c**) and PD (**d**) showing frequent immunoreactive fibers in the gland parenchyma (**a**), stroma (**b**) and around a small artery (**d**), while frequent immunoreactive puncta are seen in **c**. Lower esophagus from subjects with PD (**e, g, h**) and DLB (**f**) showing immunoreactive nerve fibers in **e**, nerve fibers and puncta in **f**, a thickened nerve fiber adherent to a bundle of smooth muscle fibers in **g** and a ganglion cell with diffuse perikaryal cytoplasmic staining in **h**

considerably through the use of multiple paraffin or 80-μm sections, such as was done for the submandibular gland and esophagus, the frequency of positive staining was increased.

For subjects with ILBD, PASH has a more limited distribution, being more likely to be confined to the spinal cord, sympathetic ganglia, vagus nerve and a subset of end-organs. Given the wide projections of the involved spinal preganglionic and sympathetic ganglion neurons, a wide but sparse involvement of the peripheral nervous system is likely to exist in ILBD, although again a more definitive investigation with multiple-section analysis will be

Table 5 Regional frequency of phosphorylated α-synuclein histopathology in single slides of different body regions, with subjects grouped by neuropathological diagnosis

Dx	SpCd	Sym	Vagus	Sciat	GI	Resp	Endo	Cardio	GU	MSK	Skin
ILBD	1/6[a]	3/6	2/7	1/6	1/7	0/4	1/4	0/6	0/4	N/A	0/2
PD	16/17	12/15	11/15	8/16	11/17[b]	1/8	2/9	0/9	1/8	0/6	0/8
DLB	9/9	7/9	4/6	2/8	5/9[c]	1/4	3/5	1/4	2/5	0/3	0/3
ADLB	1/19	2/15	1/15	0/17	1/19[d]	0/10	0/11	0/12	0/10	0/7	0/9
All	27/51	24/45	18/43	11/47	18/52	2/26	6/29	1/31	3/29	0/16	0/22

See Table 1 for listing of individual sites sampled and Fig. 4 for graphic representation; see supplementary online table for frequency of PASH within individual sites

Dx diagnosis, *SpCd* spinal cord, *Sym* sympathetic ganglia, *Vagus* vagus nerve, *Sciat* sciatic nerve, *GI* gastrointestinal system, *Resp* respiratory tract, *Endo* endocrine system, *Cardio* cardiovascular, *GU* genitourinary tract, *MSK* musculoskeletal

[a] 6/7 when multiple slides of paraffin-embedded spinal cord were examined

[b] 14/15 when multiple slides of paraffin-embedded and 80-μm frozen sections of esophagus and submandibular gland were examined

[c] 8/8 when multiple slides of paraffin-embedded and 80-μm frozen sections of esophagus and submandibular gland were examined

[d] 3/15 when multiple slides of paraffin-embedded and 80-μm frozen sections of esophagus and submandibular gland were examined

required to confirm this. Subjects with ADLB have a very restricted frequency and distribution of PASH, with very sparse involvement outside the spinal cord and sympathetic ganglia, detectable only when multiple sections are examined.

Other groups have reported higher frequencies for PASH in selected body regions including skin, adrenal medulla, urinary bladder and cardiac epicardium [35, 43, 45, 61]. Each of these earlier studies stained multiple slides from each site, however, probably accounting for most of the differences from the present work, in which for most of these regions only a single slide was stained. Differing sites of sampling may also have been responsible for differing results, for example Iwanaga et al. [45] sampled the heart from around the coronary arteries while in the present study the cardiac apex was sampled. Differences in staining methods may also have contributed to the different findings. Minguez-Castellano et al. [61] used an antibody against normal (unphosphorylated) α-synuclein while in the present study the antibody was specific for α-synuclein phosphorylated at serine 129, which is found only in pathological α-synuclein deposits [34]. Most other groups have used formic acid pretreatment for epitope exposure while the present study used proteinase K pretreatment [10, 41]. Proteinase-K would theoretically destroy normal α-synuclein and thus further eliminate non-specific (non-pathological) staining.

A critical question has been whether or not α-synuclein histopathology begins in the brain or within elements of the peripheral nervous system [20, 38, 55]. The stimulus for this intriguing hypothesis has come largely from clinical studies of PD that have found a wide range of non-motor signs and symptoms that accompany the disease [4, 78]. Many of these non-motor accompaniments are related to dysfunction of the peripheral autonomic system. These may occur early in the motor progression and there is suggestive evidence that some may even occur in the premotor prologue [2, 3, 47, 66, 74]. The description of Lewy bodies within the sympathetic and parasympathetic ganglia, adrenal medulla and GI tract within autopsied subjects with PD [17, 21, 29, 35, 39, 50, 75] has shown that peripheral nervous system α-synuclein histopathology is certainly present but there has been insufficient data regarding the findings in prodromal phases of disease. Autopsy studies of relatively small numbers of subjects with ILBD have demonstrated a high prevalence of α-synuclein histopathology within the spinal cord, sympathetic ganglia, adrenal medulla and upper GI tract [12, 17, 21, 48, 61], consistent with accumulating reports of premotor autonomic dysfunction in PD [78], but only two subjects, out of more than a thousand examined in recent studies, have had α-synuclein histopathology in the spinal cord or peripheral nervous system in the absence of brain involvement. Fumimura et al. [35] reported one case out of 783 with adrenal medulla as the only site with α-synuclein histopathology, but the olfactory bulb was not examined. Miki et al. [60] reported a single subject with α-synuclein histopathology restricted to the heart and stellate ganglion; in this case, the olfactory bulb was examined. The present work is in general agreement with these prior studies as, of the 40 subjects without brain and olfactory bulb PASH, none had PASH within the spinal cord or peripheral nervous system sites sampled. However, owing to the relatively small sample size and single-section analysis at many sites, it cannot be excluded that α-synuclein pathology may rarely begin in the peripheral nervous system prior to CNS involvement.

A derivative of the "body-first" hypothesis has been the conjecture as to whether an exogenous pathogen might be the cause of disease and gain entry through peripheral

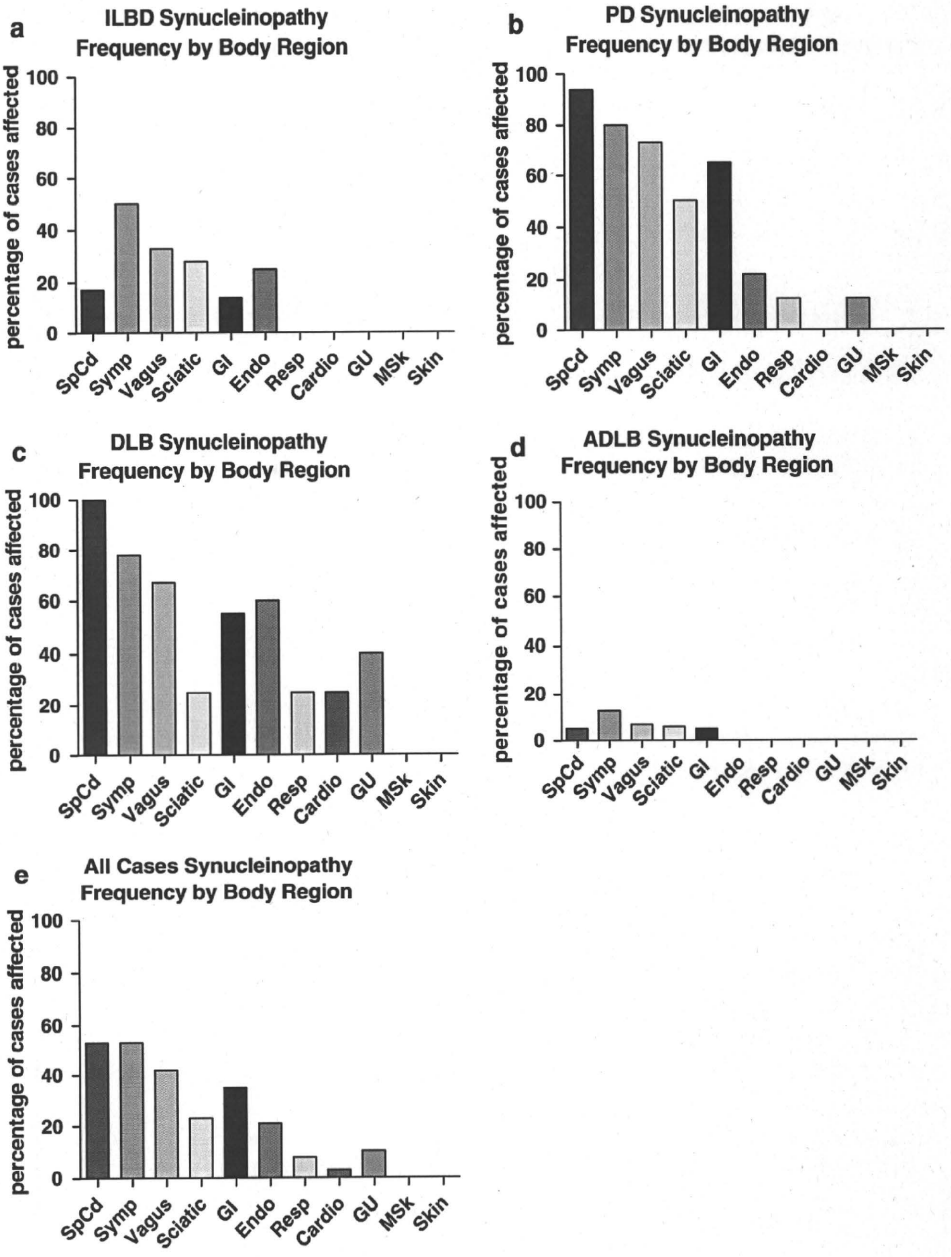

Fig. 4 Relative frequency of PASH by diagnostic group for phosphorylated α-synuclein in different body regions including spinal cord, sympathetic ganglia, vagus nerve, sciatic nerve and multiple organs and tissues. Relative frequency is the percentage of subjects that showed immunoreactive tissue elements of any kind (fibers, puncta, perikaryal diffuse staining, perikaryal cytoplasmic inclusions) in single slides from each of the sites evaluated. For list of individual sites within each body region or organ system, see Table 1 and supplementary online table. Frequency was investigated further for some sites (see text)

Table 6 Frequency and mean (SD) density of with phosphorylated α-synuclein histopathology in single slides from major spinal cord and sympathetic nervous system subdivisions (all cases considered together)

	Cervical	Thoracic	Lumbar	Sacral	CSymp	ThSymp
Frequency	23/49 (47%)	26/47 (55%)	25/49 (51%)	25/48 (52%)	14/20 (70%)	19/36 (53%)
Density score	0.7 (0.9)	1.2 (1.3)	0.9 (1.1)	1.4 (1.5)	2.1 (1.6)	1.5 (1.6)

See Fig. 5 for a graphic representation

CSymp cervical sympathetic, *ThSymp* thoracic sympathetic

nerve endings [20, 38], either through the olfactory epithelium or GI mucosa. The findings of the present study are not incompatible with a GI entry for PD, ILBD and DLB, but as subjects with ADLB have relatively rare or sparse involvement of the caudal neuraxis this seems unlikely for that group. The universal and primal involvement of the olfactory bulb in all of the Lewy body disorders [8, 11] is highly compatible with the exogenous pathogen

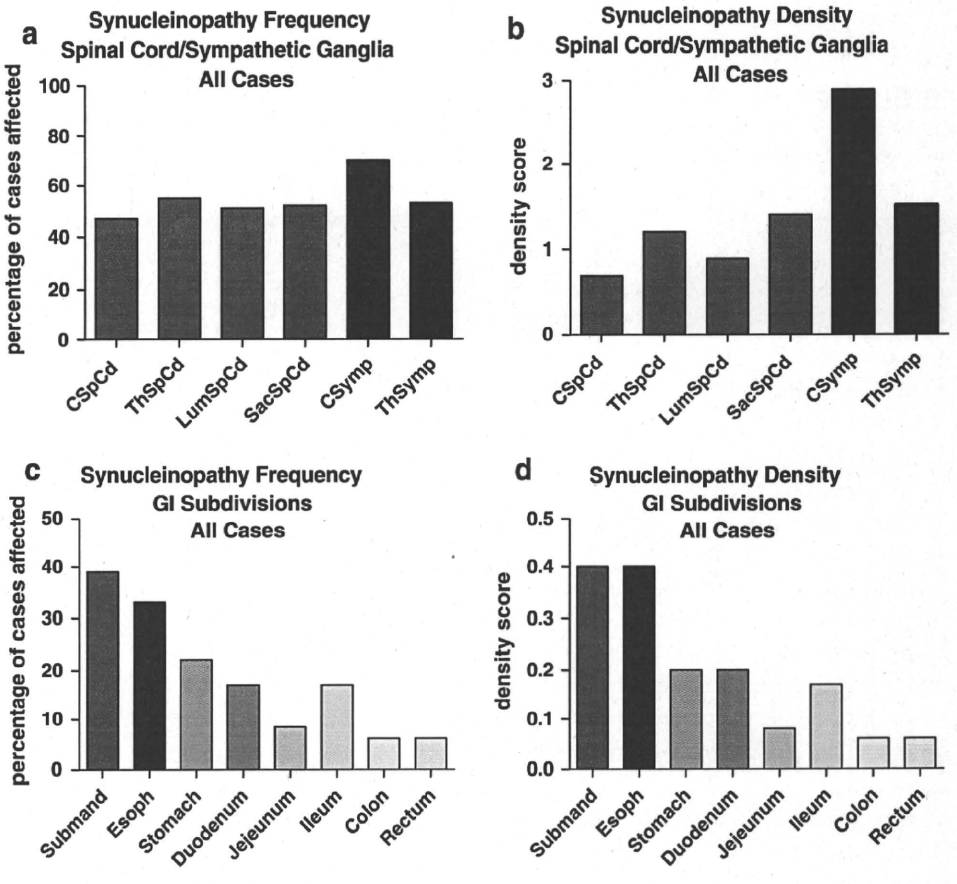

Fig. 5 Relative frequency and density of PASH by diagnostic group in different spinal cord regions and sympathetic nervous system subdivisions. Relative frequency is the percentage of subjects that showed immunoreactive tissue elements of any kind (fibers, puncta, perikaryal diffuse staining, perikaryal cytoplasmic inclusions) in single slides taken from each of the sites evaluated. Density was calculated only for sites with immunoreactivity, negative or "zero" scores were not included

Table 7 Frequency of and mean density of with phosphorylated α-synuclein histopathology in single slides of subdivisions of the gastrointestinal system (all cases considered together)

	Submand	Esoph	Stomach	Duodenum	Jejunum	Ileum	Colon	Rectum
Frequency	11/37 (39%)	17/51 (33%)	7/31 (22%)	5/30 (17%)	2/24 (8.3%)	4/24 (17%)	3/50 (6%)	3/50 (6%)
Density score	0.4 (0.7)	0.4 (0.7)	0.2 (0.4)	0.2 (0.6)	0.08 (0.28)	0.17 (0.4)	0.06 (0.2)	0.06 (0.2)

See Fig. 5 for a graphic representation

Submandib submandibular gland, *esoph* lower esophagus

hypothesis. If an exogenous pathogen is involved, whether it be a virus, micro-organism or toxin, if it was able to induce aggregation of α-synuclein in exposed neurons, this change could then be propagated throughout the remainder of the PNS and CNS, generating the observed brain and spinal cord regional pattern of α-synuclein histopathology through trans-synaptic transmission. Recently, there have been reports of PD subjects that have developed Lewy bodies within non-host neurons transplanted into the striatum more than a decade earlier, supporting the possibility that α-synuclein histopathology might be acquired and passed along from neuron to neuron [51–53, 57]. In relation to this, experimental studies have recently shown that aggregated α-synuclein may be transferred between neurons by endocytosis [26, 27, 30].

The rostrocaudal gradient of PASH within the gastrointestinal system is an interesting finding of the present work and confirms a previous report by Wakabayashi et al. [81] who mapped Lewy bodies in the alimentary tract of seven PD subjects using classical stains. The reason for this rostrocaudal gradient may be of interest. It could be due to the known distribution of vagal innervation, which extends only as far as the proximal colon and which has been documented to be more heavily distributed to the lower esophagus and stomach than to the small bowel or proximal colon [25, 42]. If so, this would suggest that, for the gastrointestinal tract, α-synuclein histopathology within vagal efferents predominates over α-synuclein histopathology originating from sympathetic ganglia or from enteric neurons. However, as Lewy bodies and α-synuclein

histopathology have been demonstrated to occur within sympathetic ganglia as well as intrinsic neurons of the enteric nervous system [17, 54, 69, 80, 81] an alternative explanation is that either or both of these have a selective rostrocaudal vulnerability to α-synuclein histopathology. A notable exception to the rostrocaudal α-synuclein histopathology gradient is the upper esophagus, which on single-slide analysis was always negative for PASH. This may be due to the fact that while most of the vagal innervation of the GI tract is derived from neuronal cell bodies located in the dorsal motor nucleus of the vagus, the cell bodies giving rise to the vagal innervation of the upper esophagus arise in the nucleus ambiguus. The former develop α-synuclein histopathology but the latter do not [20].

Spinal cord involvement with α-synuclein histopathology has usually been found to be concentrated in the preganglionic parasympathetic cell columns of the thoracolumbar intermediolateral horn and its clinical expression has, therefore, been assumed to be mainly autonomic dysfunction, but there have also been reports localizing substantial α-synuclein histopathology to the dorsal horn, where this might conceivably be a cause of neuropathic pain, and to the ventral horn, where it may affect motor neuron function [12, 21, 48, 63, 79]. The findings of the present study support these earlier works, as PASH, although most densely and frequently seen within the intermediolateral horn, was also not uncommonly present within posterior and anterior horns. The large size of some affected anterior horn neurons is consistent with involvement of small numbers of α-motor neurons, a surprising finding because there are, to our knowledge, no prior reports of Lewy bodies or α-synuclein histopathology in either spinal cord or brainstem motor neurons. Several electrophysiological studies, however, have been consistent with mild spinal motor neuron disease in PD, with evidence of motor unit reinnervation and dropout [22–24, 72, 73].

To our knowledge, this is the first report of α-synuclein histopathology within many of the sites studied. Of these, the most interesting location was the submandibular gland, which, together with the lower esophagus, was the most frequent non-neural peripheral structure affected. Sialorrhea, or drooling, has long been recognized as a characteristic sign of PD. Rather than being due to overproduction of saliva, however, sialorrhea appears to be primarily due to decreased swallowing and hence oral accumulation, and that secretion of saliva is actually decreased in subjects with PD [6, 7, 32, 56, 65, 67, 68, 76]. As both sympathetic and parasympathetic innervation of salivary glands have stimulatory effects on saliva production, it is possible that α-synuclein histopathology within either or both of these could be responsible for the decreased production observed in PD. Of further and perhaps more practical interest is the accessibility of the submandibular gland to biopsy, which could theoretically improve the low clinical diagnostic accuracy for early PD and DLB.

Acknowledgments This research is supported by Grants to the Sun Health Research Institute Brain and Body Donation Program and the Arizona Parkinson's Disease Consortium by the Michael J. Fox Foundation for Parkinson's Research (The Prescott Family Initiative), the Arizona Biomedical Research Commission (contracts 4001, 0011 and 05-901) and the National Institute on Aging (Arizona Alzheimer's Disease Consortium, P30 AG19610). We would like to thank other members of the Arizona Parkinson's Disease Consortium, including Erika Driver-Dunckley, MD, Virgilio Evidente, MD, and Donald Connor, PhD.

References

1. Consensus recommendations for the postmortem diagnosis of Alzheimer's disease (1997) The National Institute on Aging, and Reagan Institute Working Group on Diagnostic Criteria for the Neuropathological Assessment of Alzheimer's Disease Neurobiol Aging 18:S1–S2
2. Abbott RD, Petrovitch H, White LR, Masaki KH, Tanner CM, Curb JD, Grandinetti A, Blanchette PL, Popper JS, Ross GW (2001) Frequency of bowel movements and the future risk of Parkinson's disease. Neurology 57:456–462
3. Abbott RD, Ross GW, Petrovitch H, Tanner CM, Davis DG, Masaki KH, Launer LJ, Curb JD, White LR (2007) Bowel movement frequency in late-life and incidental Lewy bodies. Mov Disord
4. Adler CH (2005) Nonmotor complications in Parkinson's disease. Mov Disord 20(Suppl 11):S23–S29
5. Adler CH, Hentz JG, Joyce JN, Beach T, Caviness JN (2002) Motor impairment in normal aging, clinically possible Parkinson's disease, and clinically probable Parkinson's disease: longitudinal evaluation of a cohort of prospective brain donors. Parkinsonism Relat Disord 9:103–110
6. Bagheri H, Damase-Michel C, Lapeyre-Mestre M, Cismondo S, O'Connell D, Senard JM, Rascol O, Montastruc JL (1999) A study of salivary secretion in Parkinson's disease. Clin Neuropharmacol 22:213–215
7. Bateson MC, Gibberd FB, Wilson RS (1973) Salivary symptoms in Parkinson disease. Arch Neurol 29:274–275
8. Beach TG, Adler CH, Lue L, Sue LI, Bachalakuri J, Henry-Watson J, Sasse J, Boyer S, Shirohi S, Brooks R, Eschbacher J, White CL III, Akiyama H, Caviness J, Shill HA, Connor DJ, Sabbagh MN, Walker DG (2009) Unified staging system for Lewy body disorders: correlation with nigrostriatal degeneration, cognitive impairment and motor dysfunction. Acta Neuropathol 117:613–634
9. Beach TG, Sue LI, Walker DG, Roher AE, Lue L, Vedders L, Connor DJ, Sabbagh MN, Rogers J (2008) The Sun Health Research Institute Brain Donation Program: description and experience, 1987–2007. Cell Tissue Bank 9:229–245
10. Beach TG, White CL, Hamilton RL, Duda JE, Iwatsubo T, Dickson DW, Roncaroli F, Buttini M, Hladik CL, Sue LI, Noorigian JV, Adler CH (2008) Evaluation of alpha-synuclein immunohistochemical methods used by invited experts. Acta Neuropathol 116:277–288
11. Beach TG, White CL III, Hladik CL, Sabbagh MN, Connor DJ, Shill HA, Sue LI, Sasse J, Bachalakuri J, Henry-Watson J, Akiyama H, Adler CH (2009) Olfactory bulb alpha-synucleinopathy has high specificity and sensitivity for Lewy body disorders. Acta Neuropathol 117:169–174

12. Bloch A, Probst A, Bissig H, Adams H, Tolnay M (2006) Alpha-synuclein pathology of the spinal and peripheral autonomic nervous system in neurologically unimpaired elderly subjects. Neuropathol Appl Neurobiol 32:284–295
13. Bouras C, Hof PR, Giannakopoulos P, Michel JP, Morrison JH (1994) Regional distribution of neurofibrillary tangles and senile plaques in the cerebral cortex of elderly patients: a quantitative evaluation of a one-year autopsy population from a geriatric hospital. Cereb Cortex 4:138–150
14. Braak H, Bohl JR, Muller CM, Rub U, de Vos RA, Del Tredici K (2006) Stanley Fahn Lecture 2005: the staging procedure for the inclusion body pathology associated with sporadic Parkinson's disease reconsidered. Mov Disord 21:2042–2051
15. Braak H, Braak E (1991) Demonstration of amyloid deposits and neurofibrillary changes in whole brain sections. Brain Pathol 1:213–216
16. Braak H, Braak E (1991) Neuropathological stageing of Alzheimer-related changes. Acta Neuropathol (Berl) 82:239–259
17. Braak H, de Vos RA, Bohl J, Del Tredici K (2006) Gastric alpha-synuclein immunoreactive inclusions in Meissner's and Auerbach's plexuses in cases staged for Parkinson's disease-related brain pathology. Neurosci Lett 396:67–72
18. Braak H, Del Tredici K (2008) Invited Article: nervous system pathology in sporadic Parkinson disease. Neurology 70:1916–1925
19. Braak H, Ghebremedhin E, Rub U, Bratzke H, Del Tredici K (2004) Stages in the development of Parkinson's disease-related pathology. Cell Tissue Res 318:121–134
20. Braak H, Rub U, Gai WP, Del Tredici K (2003) Idiopathic Parkinson's disease: possible routes by which vulnerable neuronal types may be subject to neuroinvasion by an unknown pathogen. J Neural Transm 110:517–536
21. Braak H, Sastre M, Bohl JR, de Vos RA, Del Tredici K (2007) Parkinson's disease: lesions in dorsal horn layer I, involvement of parasympathetic and sympathetic pre- and postganglionic neurons. Acta Neuropathol 113:421–429
22. Brait K, Fahn S, Schwarz GA (1973) Sporadic and familial parkinsonism and motor neuron disease. Neurology 23:990–1002
23. Caviness JN, Smith BE, Clarke SJ, Adler CH, Caselli RJ, Hentz JG, Manfred MS, Muenter D (2002) Motor unit number estimates in idiopathic Parkinson's disease. Parkinsonism Relat Disord 8:161–164
24. Caviness JN, Smith BE, Stevens JC, Adler CH, Caselli RJ, Reiners CA, Hentz JG, Muenter MD (2000) Motor unit changes in sporadic idiopathic Parkinson's disease. Mov Disord 15:238–243
25. Christensen J, Stiles MJ, Rick GA, Sutherland J (1984) Comparative anatomy of the myenteric plexus of the distal colon in eight mammals. Gastroenterology 86:706–713
26. Danzer KM, Haasen D, Karow AR, Moussaud S, Habeck M, Giese A, Kretzschmar H, Hengerer B, Kostka M (2007) Different species of alpha-synuclein oligomers induce calcium influx and seeding. J Neurosci 27:9220–9232
27. Danzer KM, Krebs SK, Wolff M, Birk G, Hengerer B (2009) Seeding induced by alpha-synuclein oligomers provides evidence for spreading of alpha-synuclein pathology. J Neurochem 111:192–203
28. Del Tredici K, Rub U, de Vos RA, Bohl JR, Braak H (2002) Where does parkinson disease pathology begin in the brain? J Neuropathol Exp Neurol 61:413–426
29. den Hartog Jager WA, Bethlem J (1960) The distribution of Lewy bodies in the central and autonomic nervous systems in idiopathic paralysis agitans. J Neurol Neurosurg Psychiatry 23:283–290
30. Desplats P, Lee HJ, Bae EJ, Patrick C, Rockenstein E, Crews L, Spencer B, Masliah E, Lee SJ (2009) Inclusion formation and neuronal cell death through neuron-to-neuron transmission of alpha-synuclein. Proc Natl Acad Sci USA 106:13010–13015
31. Duda JE, Giasson BI, Mabon ME, Lee VM, Trojanowski JQ (2002) Novel antibodies to synuclein show abundant striatal pathology in Lewy body diseases. Ann Neurol 52:205–210
32. Edwards LL, Quigley EM, Harned RK, Hofman R, Pfeiffer RF (1994) Characterization of swallowing and defecation in Parkinson's disease. Am J Gastroenterol 89:15–25
33. Fujishiro H, Tsuboi Y, Lin WL, Uchikado H, Dickson DW (2008) Co-localization of tau and alpha-synuclein in the olfactory bulb in Alzheimer's disease with amygdala Lewy bodies. Acta Neuropathol 116:17–24
34. Fujiwara H, Hasegawa M, Dohmae N, Kawashima A, Masliah E, Goldberg MS, Shen J, Takio K, Iwatsubo T (2002) Alpha-synuclein is phosphorylated in synucleinopathy lesions. Nat Cell Biol 4:160–164
35. Fumimura Y, Ikemura M, Saito Y, Sengoku R, Kanemaru K, Sawabe M, Arai T, Ito G, Iwatsubo T, Fukayama M, Mizusawa H, Murayama S (2007) Analysis of the adrenal gland is useful for evaluating pathology of the peripheral autonomic nervous system in Lewy body disease. J Neuropathol Exp Neurol 66:354–362
36. Gelb DJ, Oliver E, Gilman S (1999) Diagnostic criteria for Parkinson disease. Arch Neurol 56:33–39
37. Giasson BI, Duda JE, Forman MS, Lee VM, Trojanowski JQ (2001) Prominent perikaryal expression of alpha- and beta-synuclein in neurons of dorsal root ganglion and in medullary neurons. Exp Neurol 172:354–362
38. Hawkes CH, Del Tredici K, Braak H (2007) Parkinson's disease: a dual-hit hypothesis. Neuropathol Appl Neurobiol 33:599–614
39. Hishikawa N, Hashizume Y, Hirayama M, Imamura K, Washimi Y, Koike Y, Mabuchi C, Yoshida M, Sobue G (2000) Brainstem-type Lewy body disease presenting with progressive autonomic failure and lethargy. Clin Auton Res 10:139–143
40. Hishikawa N, Hashizume Y, Yoshida M, Sobue G (2003) Clinical and neuropathological correlates of Lewy body disease. Acta Neuropathol 105:341–350
41. Hladik CL, White CL (2003) Comparison of digestive enzyme and formic acid pretreatment for optimal immunohistochemical demonstration of alpha-synuclein-immunoreactive cerebral cortical Lewy neurites. J Neuropathol Exp Neurol 62:554
42. Hopkins DA, Bieger D, deVente J, Steinbusch WM (1996) Vagal efferent projections: viscerotopy, neurochemistry and effects of vagotomy. Prog Brain Res 107:79–96
43. Ikemura M, Saito Y, Sengoku R, Sakiyama Y, Hatsuta H, Kanemaru K, Sawabe M, Arai T, Ito G, Iwatsubo T, Fukayama M, Murayama S (2008) Lewy body pathology involves cutaneous nerves. J Neuropathol Exp Neurol 67:945–953
44. Iseki E, Marui W, Kosaka K, Akiyama H, Ueda K, Iwatsubo T (1998) Degenerative terminals of the perforant pathway are human alpha-synuclein-immunoreactive in the hippocampus of patients with diffuse Lewy body disease. Neurosci Lett 258:81–84
45. Iwanaga K, Wakabayashi K, Yoshimoto M, Tomita I, Satoh H, Takashima H, Satoh A, Seto M, Tsujihata M, Takahashi H (1999) Lewy body-type degeneration in cardiac plexus in Parkinson's and incidental Lewy body diseases. Neurology 52:1269–1271
46. Jellinger KA (2004) Lewy body-related alpha-synucleinopathy in the aged human brain. J Neural Transm 111:1219–1235
47. Kaufmann H, Nahm K, Purohit D, Wolfe D (2004) Autonomic failure as the initial presentation of Parkinson disease and dementia with Lewy bodies. Neurology 63:1093–1095
48. Klos KJ, Ahlskog JE, Josephs KA, Apaydin H, Parisi JE, Boeve BF, DeLucia MW, Dickson DW (2006) Alpha-synuclein pathology in the spinal cords of neurologically asymptomatic aged individuals. Neurology 66:1100–1102
49. Knowles CH, De GR, Kapur RP, Bruder E, Farrugia G, Geboes K, Gershon MD, Hutson J, Lindberg G, Martin JE, Meier-Ruge WA, Milla PJ, Smith VV, Vandervinden JM, Veress B, Wedel T

(2009) Gastrointestinal neuromuscular pathology: guidelines for histological techniques and reporting on behalf of the Gastro 2009 International Working Group. Acta Neuropathol 118:271–301
50. Koike Y, Takahashi A (1997) Autonomic dysfunction in Parkinson's disease. Eur Neurol 38(Suppl 2):8–12
51. Kordower JH, Brundin P (2009) Lewy body pathology in long-term fetal nigral transplants: is Parkinson's disease transmitted from one neural system to another? Neuropsychopharmacology 34:254
52. Kordower JH, Chu Y, Hauser RA, Freeman TB, Olanow CW (2008) Lewy body-like pathology in long-term embryonic nigral transplants in Parkinson's disease. Nat Med 14:504–506
53. Kordower JH, Chu Y, Hauser RA, Olanow CW, Freeman TB (2008) Transplanted dopaminergic neurons develop PD pathologic changes: a second case report. Mov Disord 23:2303–2306
54. Kupsky WJ, Grimes MM, Sweeting J, Bertsch R, Cote LJ (1987) Parkinson's disease and megacolon: concentric hyaline inclusions (Lewy bodies) in enteric ganglion cells. Neurology 37:1253–1255
55. Langston JW (2006) The Parkinson's complex: parkinsonism is just the tip of the iceberg. Ann Neurol 59:591–596
56. Leopold NA, Kagel MC (1997) Pharyngo-esophageal dysphagia in Parkinson's disease. Dysphagia 12:11–18
57. Li JY, Englund E, Holton JL, Soulet D, Hagell P, Lees AJ, Lashley T, Quinn NP, Rehncrona S, Bjorklund A, Widner H, Revesz T, Lindvall O, Brundin P (2008) Lewy bodies in grafted neurons in subjects with Parkinson's disease suggest host-to-graft disease propagation. Nat Med 14:501–503
58. McKeith IG, Dickson DW, Lowe J, Emre M, O'Brien JT, Feldman H, Cummings J, Duda JE, Lippa C, Perry EK, Aarsland D, Arai H, Ballard CG, Boeve B, Burn DJ, Costa D, Del ST, Dubois B, Galasko D, Gauthier S, Goetz CG, Gomez-Tortosa E, Halliday G, Hansen LA, Hardy J, Iwatsubo T, Kalaria RN, Kaufer D, Kenny RA, Korczyn A, Kosaka K, Lee VM, Lees A, Litvan I, Londos E, Lopez OL, Minoshima S, Mizuno Y, Molina JA, Mukaetova-Ladinska EB, Pasquier F, Perry RH, Schulz JB, Trojanowski JQ, Yamada M (2005) Diagnosis and management of dementia with Lewy bodies: third report of the DLB Consortium. Neurology 65:1863–1872
59. McKeith IG, Galasko D, Kosaka K, Perry EK, Dickson DW, Hansen LA, Salmon DP, Lowe J, Mirra SS, Byrne EJ, Lennox G, Quinn NP, Edwardson JA, Ince PG, Bergeron C, Burns A, Miller BL, Lovestone S, Collerton D, Jansen EN, Ballard C, de Vos RA, Wilcock GK, Jellinger KA, Perry RH (1996) Consensus guidelines for the clinical and pathologic diagnosis of dementia with Lewy bodies (DLB): report of the consortium on DLB international workshop. Neurology 47:1113–1124
60. Miki Y, Mori F, Wakabayashi K, Kuroda N, Orimo S (2009) Incidental Lewy body disease restricted to the heart and stellate ganglia. Mov Disord 24:2299–2301
61. Minguez-Castellanos A, Chamorro CE, Escamilla-Sevilla F, Ortega-Moreno A, Rebollo AC, Gomez-Rio M, Concha A, Munoz DG (2007) Do alpha-synuclein aggregates in autonomic plexuses predate Lewy body disorders? A cohort study. Neurology 68:2012–2018
62. Mirra SS, Heyman A, McKeel D, Sumi SM, Crain BJ, Brownlee LM, Vogel FS, Hughes JP, van Belle G, Berg L (1991) The Consortium to Establish a Registry for Alzheimer's Disease (CERAD). Part II. Standardization of the neuropathologic assessment of Alzheimer's disease. Neurology 41:479–486
63. O'Sullivan SS, Holton JL, Massey LA, Williams DR, Revesz T, Lees AJ (2008) Parkinson's disease with Onuf's nucleus involvement mimicking multiple system atrophy. J Neurol Neurosurg Psychiatry 79:232–234
64. Parkkinen L, Pirttila T, Alafuzoff I (2008) Applicability of current staging/categorization of alpha-synuclein pathology and their clinical relevance. Acta Neuropathol 115:399–407
65. Persson M, Osterberg T, Granerus AK, Karlsson S (1992) Influence of Parkinson's disease on oral health. Acta Odontol Scand 50:37–42
66. Pfeiffer RF (2003) Gastrointestinal dysfunction in Parkinson's disease. Lancet Neurol 2:107–116
67. Pinnington LL, Muhiddin KA, Ellis RE, Playford ED (2000) Non-invasive assessment of swallowing and respiration in Parkinson's disease. J Neurol 247:773–777
68. Proulx M, de Courval FP, Wiseman MA, Panisset M (2005) Salivary production in Parkinson's disease. Mov Disord 20:204–207
69. Qualman SJ, Haupt HM, Yang P, Hamilton SR (1984) Esophageal Lewy bodies associated with ganglion cell loss in achalasia. Similarity to Parkinson's disease. Gastroenterology 87:848–856
70. Saito Y, Kawashima A, Ruberu NN, Fujiwara H, Koyama S, Sawabe M, Arai T, Nagura H, Yamanouchi H, Hasegawa M, Iwatsubo T, Murayama S (2003) Accumulation of phosphorylated alpha-synuclein in aging human brain. J Neuropathol Exp Neurol 62:644–654
71. Saito Y, Ruberu NN, Sawabe M, Arai T, Kazama H, Hosoi T, Yamanouchi H, Murayama S (2004) Lewy body-related alpha-synucleinopathy in aging. J Neuropathol Exp Neurol 63:742–749
72. Sica RE, Herskovits E, Aguilera N, Poch G (1973) An electrophysiological investigation of skeletal muscle in Parkinson's disease. J Neurol Sci 18:411–420
73. Sica RE, Sanz OP (1976) An electrophysiological study of the functional changes in the spinal motoneurones in Parkinson's disease. Electromyogr Clin Neurophysiol 16:409–417
74. Siddiqui MF, Rast S, Lynn MJ, Auchus AP, Pfeiffer RF (2002) Autonomic dysfunction in Parkinson's disease: a comprehensive symptom survey. Parkinsonism Relat Disord 8:277–284
75. Takeda S, Yamazaki K, Miyakawa T, Arai H (1993) Parkinson's disease with involvement of the parasympathetic ganglia. Acta Neuropathol 86:397–398
76. Tumilasci OR, Cersosimo MG, Belforte JE, Micheli FE, Benarroch EE, Pazo JH (2006) Quantitative study of salivary secretion in Parkinson's disease. Mov Disord 21:660–667
77. Uchikado H, Lin WL, DeLucia MW, Dickson DW (2006) Alzheimer disease with amygdala Lewy bodies: a distinct form of alpha-synucleinopathy. J Neuropathol Exp Neurol 65:685–697
78. Verbaan D, Marinus J, Visser M, van Rooden SM, Stiggelbout AM, van Hilten JJ (2007) Patient-reported autonomic symptoms in Parkinson disease. Neurology 69:333–341
79. Wakabayashi K, Takahashi H (1997) The intermediolateral nucleus and Clarke's column in Parkinson's disease. Acta Neuropathol 94:287–289
80. Wakabayashi K, Takahashi H, Ohama E, Ikuta F (1990) Parkinson's disease: an immunohistochemical study of Lewy body-containing neurons in the enteric nervous system. Acta Neuropathol 79:581–583
81. Wakabayashi K, Takahashi H, Takeda S, Ohama E, Ikuta F (1988) Parkinson's disease: the presence of Lewy bodies in Auerbach's and Meissner's plexuses. Acta Neuropathol 76:217–221
82. Zaccai J, Brayne C, McKeith I, Matthews F, Ince PG (2008) Patterns and stages of alpha-synucleinopathy: relevance in a population-based cohort. Neurology 70:1042–1048

Modeling familial Danish dementia in mice supports the concept of the amyloid hypothesis of Alzheimer's disease

Janaky Coomaraswamy[a,b,1], Ellen Kilger[a,b], Heidrun Wölfing[a,b,c], Claudia Schäfer[a,b], Stephan A. Kaeser[a,b], Bettina M. Wegenast-Braun[a,b,c], Jasmin K. Hefendehl[a,b,c], Hartwig Wolburg[d], Matthew Mazzella[e], Jorge Ghiso[f], Michel Goedert[g], Haruhiko Akiyama[h], Francisco Garcia-Sierra[i], David P. Wolfer[j], Paul M. Mathews[e,f], and Mathias Jucker[a,b,1]

[a]Department of Cellular Neurology, Hertie-Institute for Clinical Brain Research, [c]Graduate School of Cellular and Molecular Neuroscience, and [d]Department of Pathology, University of Tübingen, 72076 Tübingen, Germany; [b]German Center for Neurodegenerative Diseases, 72076 Tübingen, Germany; [e]Nathan Kline Institute, Orangeburg, New York, NY 10962; [f]New York University School of Medicine, New York, NY 10016; [g]Medical Research Council Laboratory of Molecular Biology, Cambridge CB2 2QH, United Kingdom; [h]Tokyo Institute of Psychiatry, 156-8585 Tokyo, Japan; [i]Department of Cell Biology, Center of Research and Advanced Studies of the National Polytechnic Institute, CP 07360 Mexico City, Mexico; and [j]Institute of Anatomy and Center for Integrative Human Physiology, University of Zürich, and Human Movement Sciences, Swiss Federal Institute of Technology, CH-8057 Zürich, Switzerland

Edited by Thomas C. Südhof, Stanford University School of Medicine, Palo Alto, CA, and approved March 16, 2010 (received for review January 31, 2010)

Familial Danish dementia (FDD) is a progressive neurodegenerative disease with cerebral deposition of Dan-amyloid (ADan), neuroinflammation, and neurofibrillary tangles, hallmark characteristics remarkably similar to those in Alzheimer's disease (AD). We have generated transgenic (tg) mouse models of familial Danish dementia that exhibit the age-dependent deposition of ADan throughout the brain with associated amyloid angiopathy, microhemorrhage, neuritic dystrophy, and neuroinflammation. Tg mice are impaired in the Morris water maze and exhibit increased anxiety in the open field. When crossed with TauP301S tg mice, ADan accumulation promotes neurofibrillary lesions, in all aspects similar to the Tau lesions observed in crosses between β-amyloid (Aβ)-depositing tg mice and TauP301S tg mice. Although these observations argue for shared mechanisms of downstream pathophysiology for the sequence-unrelated ADan and Aβ peptides, the lack of codeposition of the two peptides in crosses between ADan- and Aβ-depositing mice points also to distinguishing properties of the peptides. Our results support the concept of the amyloid hypothesis for AD and related dementias, and suggest that different proteins prone to amyloid formation can drive strikingly similar pathogenic pathways in the brain.

ADan | ABeta | tau | neurodegeneration | mouse model

Familial Danish dementia (FDD) is an autosomal-dominant disorder caused by a 10 nucleotide duplication just before the stop codon of the *BRI2* gene (also known as *ITM2B*) (1). This mutation generates an extended ORF, resulting in expression of a C-terminally elongated protein. The BRI2-type II integral transmembrane protein is processed by furin-like protease (2, 3), and through this normal processing the FDD mutation results in the release of the longer than normal and amyloidogenic C-terminal cleavage product designated Dan-amyloid (ADan) (represented in Fig. 1*A*). Similar to many other neurodegenerative diseases, FDD is a disease involving aberrant protein accumulation. Certain features of the disease pathology, such as the accumulation of the ADan peptide as widespread cerebral vascular amyloid and abundant amyloid plaques in the hippocampus, as well as the associated neurofibrillary Tau pathology and neuroinflammation, are remarkably similar to those seen in Alzheimer's disease (AD) (4). The clinical course of disease includes progressive dementia; however, it also features visual cataracts, hearing loss, spasticity, and cerebellar ataxia (4).

The amyloid hypothesis of AD—which may be extended to similar amyloidoses, such as FDD—stresses the role of increased amyloidogenic peptide levels and amyloid formation as a causative factor in instigating disease pathogenesis (5). This hypothesis is strongly supported by the effects of the mutations that lead to familial forms of AD. Indeed, many transgenic (tg) mouse models of AD recapitulating cerebral β-amyloidosis (Aβ) and associated lesions, neuroinflammation, and memory impairment, are based on familial AD mutations that increase Aβ production (6–9). However, the majority of AD cases are sporadic and challenges have been raised to the amyloid hypothesis by arguing that the increase in Aβ plaque pathology and neurofibrillary tangle formation may be linked through parallel but independent mechanisms (10). Additionally, Aβ deposition and tangle formation may be disease bystanders rather than causative for the disease (11).

To advance our understanding of FDD pathogenesis, we generated tg mice that overexpress the Danish mutant form of BRI2 (ADan precursor protein; ADanPP). By cross-breeding these mice, we have examined the relationship between ADan- and Aβ pathology and the impact of ADan on the promotion of Tau pathology.

Results

ADanPP-Tg Mice Demonstrate the Age-Related Deposition of ADan. Tg mice expressing the Danish mutant form of BRI2 (Fig. 1*A*) were generated on a C57BL/6 background using the cosmid-based Syrian Hamster prion protein expression cassette. Two tg lines were selected (ADanPP6 and ADanPP7). The ADanPP7 line revealed higher levels of both full-length and cleaved precursor protein expression compared with the ADanPP6 line, and several-fold that over endogenous murine Bri2 (Fig. 1*B*). The ADanPP7 mice were then analyzed more extensively.

Precursor protein expression in ADanPP7 mice remains stable with aging; however, ADan peptide is initially detected by routine Western blotting at 4 months of age and increases dramatically with aging (Fig. 1*C*). Immunohistochemical analysis revealed ADanPP expression throughout the brain, mainly in neurons and to a lesser degree in astrocytes, with the strongest staining in hippocampus and neocortex (Fig. 1*D*). As early as 2 months of age, ADan deposition, detected by immunohistochemistry or amyloid-binding dyes (thioflavin S, Congo red, methoxy), was observed in

Author contributions: J.C., F.G-S., D.P.W., P.M.M., and M.J. designed research; J.C., E.K., H. Wölfing, C.S., S.A.K., B.M.W.-B., J.K.H., H. Wolburg, M.M., F.G.-S., and D.P.W. performed research; J.G., M.G., and H.A. contributed new reagents/analytic tools; J.C., E.K., H. Wölfing, S.A.K., B.M.W.-B., J.K.H., H. Wolburg, M.M., F.G.-S., D.P.W., P.M.M., and M.J. analyzed data; and J.C., F.G.-S., D.P.W., P.M.M., and M.J. wrote the paper.

The authors declare no conflict of interest.

This article is a PNAS Direct Submission.

[1]To whom correspondence may be addressed. E-mail: janaky.coomaraswamy@uni-tuebingen.de or mathias.jucker@uni-tuebingen.de.

This article contains supporting information online at www.pnas.org/cgi/content/full/1001056107/DCSupplemental.

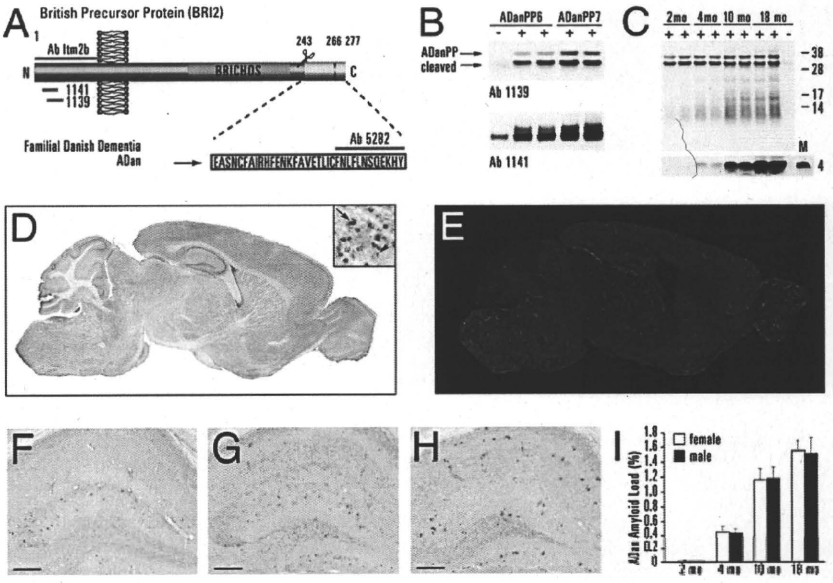

Fig. 1. Age-related deposition of cerebral Dan-amyloid in ADanPP-tg mice. (*A*) Mutant *BRI2* contains a 10-nucleotide duplication just before the stop codon generating a longer ORF (277 instead of 266 amino acids) (1). Normal cleavage at position 243 by a furin-like protease releases the amyloidogenic 34 amino acid long ADan peptide in FDD (2, 3). In addition, BRI2 undergoes processing by ADAM10 to release the extracellular Brichos domain from the membrane-bound N-terminal part that, in turn, undergoes regulated intramembrane proteolysis by SPPL2a/b (42). The recognition sites of various antibodies (Ab) are indicated in green. (*B*) Western blotting at 2 months of age reveals higher levels of ADanPP in line 7 compared to line 6 (*Upper*, Ab 1139). Transgene expression in line 7 is several-fold higher than endogenous murine Itm2b (*Lower*, Ab 1141 recognizes both murine and human BRI2). (*C*) Western blot of ADanPP7 mouse brain at 2, 4, 10, and 18 months demonstrates that levels of precursor protein remain relatively the same (*Upper*, Ab 1139) with increasing accumulation of ADan peptide, which runs at the same height as the ADan monomer (M) of FDD patients (*Lower*, Ab 5282). (*D*) ADanPP expression in a 2-month-old ADanPP7 mouse (Ab Itm2b). (*E*) Methoxy staining of ADan lesions in an 18-month-old ADanPP7 mouse. (*F–I*) Quantification of the amyloid lesions in ADanPP7 mice in hippocampus was done using ADan-specific Ab 5282 in combination with Congo red. At 4 months of age amyloid deposits are seen in the stratum lacunosum moleculare of CA3 (*F*); at 10 months of age the amyloid appears largely associated with vessels and occurs throughout the dentate gyrus (*G*); at 18 months of age the entire hippocampus is covered with amyloid lesions (*H*). Stereological analysis of the Congo-red ADan material (*I*) revealed a significant increase from 2 to 18 months of age [$F(3,24) = 56.404$, $P < 0.0001$] with no gender difference [$F(1,24) = 0.017$, $P = 0.8979$; $n = 4$ females and 4 males, per age group]. (Scale bar, 200 μm.)

hippocampus and in meningeal vessels. At 18 months of age, ADan deposition occurs throughout the brain (Fig. 1*E*), including the amygdala, thalamus, brainstem, and to a lesser extent the cerebellum, with the majority of ADan-deposits associated with the vasculature. Stereological quantification in the hippocampus of 2-, 4-, 10-, and 18-month-old ADanPP7 mice confirmed the age-related increase in ADan deposition, which starts in the stratum lacunosum moleculare of the CA3 region, followed by the dentate gyrus and the CA1 region. ADan accumulation did not significantly differ between genders (Fig. 1 *F–I*). ADan deposition in the ADanPP6 line showed a delayed progression compared to the ADanPP7 line, but generally followed a similar distribution.

ADan Lesions and Their Impact on the Neuropil and Vasculature. ADan deposition was primarily associated with the vasculature. Although in larger vessels the ADan was confined to the vessel wall with a sheet-like appearance (Fig. 2*A*), other smaller vessels revealed a thick coat of ADan that often completely obstructed the vessel lumen (Fig. 2*B*). Perivascular plaques often surrounded a significant portion of the vessel surface, and appeared as parenchymal plaque-like structures (Fig. 2*C*). Some lesions appearing to be parenchymal ADan deposits (Fig. 2*D*) were typically surrounded by a cloud of small punctate ADan-immunoreactive, but Congo red-negative, aggregates. By 18 months of age, entire regions—including the hippocampus, cortex, and brainstem—were covered with diffuse clouds of the small punctate ADan-immunoreactive aggregates.

Ultrastructural analysis revealed that ADan is highly compact in nature (Fig. 2 *E–G*). Amyloid in the vessel wall appeared to be integrated into the endothelial and vascular basement membrane and lead to an abnormal thickening of the membrane and destruction of vessel wall integrity (Fig. 2*E*). Often, such perivascular amyloid penetrated into the surrounding parenchyma and was found to be surrounded by microglia and dystrophic neurites (Fig. 2*F*). Smaller "plaque-like" lesions without an obvious vascular component were also observed, typically surrounded by microglial cytosolic structures (Fig. 2*G*).

With age, the accumulation of ADan in the vasculature led to a loss of vascular smooth-muscle cells (Fig. 2 *H* and *I*). Consistent with a weakening of the vessel wall, vessel-associated microbleeds were observed in the 18-month-old ADanPP7 tg mice, although no incidence of microhemorrhage was found in the control non-tg mice (Fig. 2 *J* and *K*).

Associated primarily with parenchymal ADan lesions, dystrophic boutons were detected (Fig. 2*L*), an observation consistent with the ultrastructural analysis (Fig. 2*F*). Additionally, structures consistent with (secondary) axonal swelling or spheroids were observed throughout the brain in regions with ADan deposition (Fig. 2*L*). No significant neuron loss was found in the hippocampus, although there was an apparent displacement of neuronal cell bodies in the CA3/4 region of the hippocampus (Fig. 2 *M–O*).

ADan Lesions Evoke a Neuroinflammatory Response. ADan deposition elicited a robust activation of astrocytes, revealed by darkly stained GFAP-immunoreactive hypertrophic cell bodies and processes (Fig. 3 *A–F*). Astrocytosis, initially seen in the stratum lacunosum moleculare of the CA3 hippocampal region (Fig. 3*D*), spread throughout the hippocampus and neocortex, and closely followed the temporal pattern of ADan deposition (Fig. 3*E*). By 18 months of age, astrogliosis was seen throughout the entire brain (Fig. 3*F*). Similarly, microgliosis closely followed the spreading and temporal development of the amyloid lesions (Fig. 3 *G–L*). Although activated astrocytes covered entire areas containing ADan deposits with hypertrophic processes (Fig. 3*M*), activated microglia were observed in close juxtaposition to amyloid deposits, with one to four microglial cells per ADan deposit (Fig. 3*N*). Confocal microscopy confirmed the tight association between microglia and ADan deposits (Fig. 3*O*).

ADanPP Mice Have Behavioral Deficits, Including Increased Anxiety. In the place and cue navigation task of the Morris water maze, 18- to 20-month-old ADanPP7 mice took longer to find the platform compared with age-matched non-tg controls (Fig. S1*A*). When the swim path was analyzed, a flattened learning curve was found (Fig. S1*B*). Thigmotaxis and passive floating were increased in the tg mice; however, swim speed was reduced (Fig. S1). During the probe trials, tg mice tended to have a lower preference for the

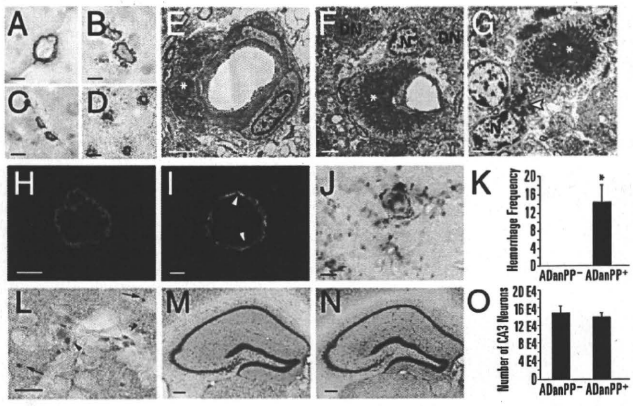

Fig. 2. ADan lesions and their impact on the neuropil and vasculature. (*A–D*) Various types of ADan lesions in 18-month-old ADanPP7 tg mice (Ab 5282) at light microscopic level. (*E–G*) Ultrastructural appearance of the ADan lesions. Amyloid fibrils (asteriks), microglia cell nucleus (N); dystrophic neurites (DN); microglia cell with the typical features of phagosomal/lysosomal material (arrowhead in *G*). (*H* and *I*) Confocal microscopy of double-immunolabeled vessels (red, smooth muscle-cell actin; green, ADan) in a non-tg control (*H*) and tg (*I*) mouse. Note the focal disappearance of smooth muscle cells at sites of ADan deposition (arrowheads, *I*). (*J*) Hemosiderin-positive microglia (blue) reveal the occurrence of cerebral microhemorrhages. (*K*) Hemorrhage frequency per hemisphere in tg and non-tg 18-month-old mice [$F(1,14) = 14.440$, $P < 0.002$; $n = 8$, four females and four males per group). (*L*) Dystrophic synaptophysin-positive structures in the vicinity of both parenchymal and vascular ADan deposits (arrowhead), but also throughout the parenchyma (arrow). (*M* and *N*) Cresyl violet staining of the hippocampus of an 18-month-old tg mouse (*N*) compared with a non-tg littermate (*M*). (*O*) Number of CA3 neurons in 18-month-old ADanPP7 mice did not reveal significant changes [$F(1,10) = 0.326$, $P = 0.5806$; $n = 6$ non-tg, 6 tg; five males, seven females). [Scale bars: 20 μm (*A–D, J, L*), 2 μm (*E, G*), 3 μm (*F*), 10 μm (*H, I*), 200 μm (*M, N*).]

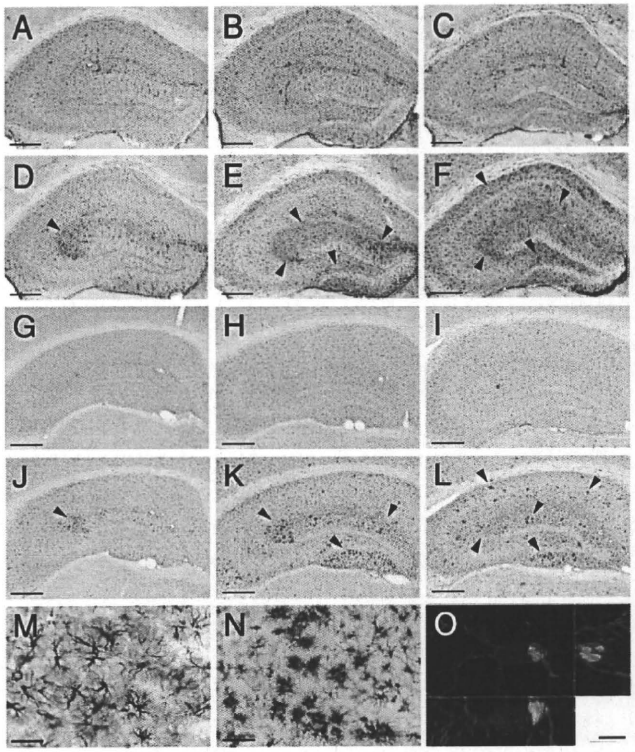

Fig. 3. Glial activation in response to ADan deposition. (*A–F*) GFAP immunohistochemistry reveals an activation of astrocytes (arrowheads) at sites of Congo-red stained ADan deposition (red) in 4-month-old (*D*), 10-month-old (*E*), and 18-month-old (*F*) ADanPP7 tg mice. No such hypertrophic and darkly stained astrocytes are seen in non-tg littermates (*A, B,* and *C,* respectively). (*G–L*) Similarly, activation of Iba1-positive microglia in ADanPP7 mice closely follows the temporal-spatial pattern of ADan deposition (arrowheads in *J, K,* and *L*). Corresponding non-tg littermates in (*G, H,* and *I,* respectively). (*M* and *N*) Higher magnification of $GFAP^+$ astroglia (*M*) and $Iba1^+$ microglia (*N*) with congophillic amyloid (red). (*O*) Confocal imaging of Iba1 (red) and amyloid (green; methoxy staining) gives the impression that microglia are capable of engulfing ADan (shown is a *z*-stack of 28 slices). [Scale bars: 300 μm (*A–L*), 50 μm (*M* and *N*), 5 μm (*O*).]

trained target zone compared with the controls (Fig. S1 *C* and *D*). Searching precision during the two probe trials revealed a minor reduction after 24 h, and a total loss of spatial selectivity after 6 d (Fig. S1 *E* and *F*).

In the open field, the ADanPP7 mice revealed reduced activity in the beginning of each of the two observation periods (Fig. S1*G*). This observation, together with the increased preference of tg mice for the wall zone (Fig. S1*H*), the observed reduction of vertical activity, and the more numerous fecal boli in the open field (Fig. S1), is indicative of an anxiety-related phenotype of the ADanPP7 mice.

At 6 months of age, ADanPP7 mice did not display the phenotypic changes that were observed in the aged mice, suggesting that the behavioral changes in the ADanPP7 mice are age-dependent (Fig. S1).

Analysis of body weight revealed that ADanPP7 tg mice failed to gain weight with age (Fig. S1*I*). This failure to continue to gain weight is temporally coincident with brain amyloid accumulation. By 18 months of age, the ADanPP7 mice were 20 to 30% lighter than their non-tg littermates, and additionally showed alopecia and kyphosis.

Aβ Deposition Is Reduced and Not Coincident with ADan Deposition in Double-Tg ADanPP7/APPPS1 Mice. The Aβ and ADan peptides have been reported to colocalize in amyloid lesions of FDD patients, suggesting a disease-promoting pathogenic interaction (4, 12, 13). To examine this, ADanPP7 mice were crossed with Aβ-depositing APPPS1 tg mice (14) and analyzed at 4 months of age, when single-tg mice exhibit ADan and Aβ deposits, respectively. Surprisingly, double-tg ADanPP7/APPPS1 mice showed a 68% reduction in neocortical Aβ deposition compared with APPPS1 single-tg littermates (Fig. 4 *A–C*). Western blot of whole-brain homogenates confirmed a decrease in both Aβ40 and Aβ42 in double-tg mice compared with single-tg APPPS1 mice, while levels of amyloid precursor protein (APP) remained relatively unchanged (Fig. 4 *D–F*). In contrast to Aβ, ADan levels were not different between double-tg ADanPP7/APPPS1 and single-tg ADanPP7 littermates (Fig. 4 *G–I*). Immunohistochemical analysis of ADan deposition also showed no appreciable difference between double-tg ADanPP7/APPPS1 and single-tg ADanPP7 mice. Given that BRI2 expression has been shown to alter APP metabolism and Aβ generation (15–18), brain Aβ levels were determined in 1.5-month-old predepositing mice. A small, but not statistically significant, decrease (15–17%) in both Aβ40 and Aβ42 was seen comparing double-tg mice with single-tg APPPS1 littermates [Aβ40: 0.72 ± 0.21 and 0.60 ± 0.08 pmol/g wet weight; $F(1,14) = 0.466$, $P = 0.506$; Aβ42: 0.97 ± 0.19 and 0.82 ± 0.09 pmol/g; $F(1,14) = 0.686$, $P = 0.421$; $n = 5$ single tg, 11 double tg; all females]. To confirm the reduction in Aβ pathology by ADanPP/ADan and to eliminate any confound because of the high Aβ42-drive from the PS1 mutation in the APPPS1 line, the lower-expressing ADanPP6 line was crossed with the APP23 mouse model (9). At 13 months of age, again when single-tg mice exhibit ADan and Aβ deposits, a 70.0% reduction in Aβ deposition in the neocortex of double-tg ADanPP6/APP23 mice was seen compared to single-tg APP23 mice [$0.42 \pm 0.11\%$ vs. $1.41 \pm 0.42\%$ Aβ load; $n = 6$ and 4 per group; all females; $F(1,8) = 7.734$, $P < 0.03$].

Double immunolabeling of sections from both ADanPP7/APPPS1 mice and ADanPP6/APP23 mice showed limited coincidence of the two amyloids. Although ADan and Aβ appeared to

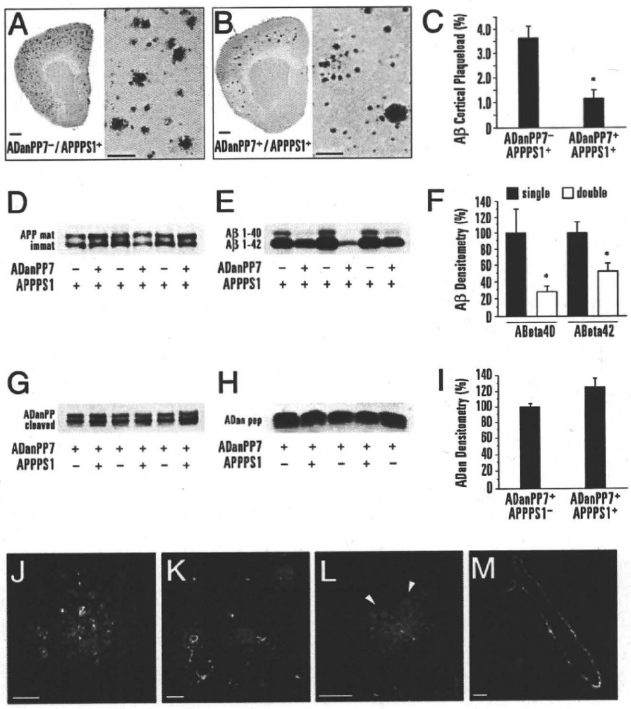

Fig. 4. Aβ deposition is reduced and not coincident with ADan deposition in double-tg ADanPP7/APPPS1 mice. (*A* and *B*) Aβ immunostaining of 4-month-old ADanPP7$^+$/APPPS1$^+$ double-tg mice compared with single-tg ADanPP7$^-$/APPPS1$^+$ littermates reveals a decrease in Aβ deposition. Higher magnifications additionally show a change in plaque morphology (i.e., less but occasionally larger plaques in the double-tg mice). (*C*) Quantification of neocortical Aβ load reveals a drastic decrease in Aβ deposition in the double-tg mice [$F(1,10) = 17.852$, $P < 0.0019$; all females; $n = 5$ single tg, $n = 7$ double tg]. (*D* and *E*) Western blotting of APP and Aβ40/42 (Ab 6E10) in ADanPP7$^+$/APPPS1$^+$ mice in comparison with ADanPP7$^-$/APPPS1$^+$ siblings reveals no change in APP but a decrease in the double-tg mice in both Aβ40 and Aβ42. Shown are three mice from each genotype. (*F*) Densitometry of Aβ levels of all of the mice confirms the significant decrease in both Aβ40 [71.4%, $F(1,10) = 7.444$, $P < 0.0213$] and Aβ42 [47.9%, $F(1,10) = 8.106$, $P < 0.0173$] species (all females; $n = 5$ single tg, 7 double tg). (*G* and *H*) Western blotting of ADanPP (Ab Itm2b) and ADan peptide (Ab 5282) reveals no change in ADanPP and ADan levels between genotypes. Shown are three mice each. (*I*) Densitometry of ADan levels of all of the mice indicates no significant difference (all females; $n = 4$ single tg, 7 double tg). (*J–M*) Confocal microscopy reveals deposition of both peptides (green, ADan; red, Aβ) in some amyloid plaques in the neocortex of double-tg mice; however, plaques consistently contained separate amyloid foci in which the two proteins do not colocalize (*J*). Other amyloid deposits in the hippocampus demonstrated deposition of only ADan or only Aβ in close vicinity to each other (*K*). Plaques consisting of only Aβ were often decorated with ADanPP/ADan$^+$ dystrophic boutons (arrowheads in *L*). Vascular amyloid consistently contained either ADan alone, or fascinatingly, both ADan and Aβ as separate foci along the same vessel, without colocalization. [Scale bars: 500 and100 μm (*A* and *B*), and 20 μm (*J–M*).]

coexist in individual amyloid plaques, they formed separate foci within a given plaque (Fig. 4*J*). More interestingly, a large portion of plaques consisted of only one amyloid peptide (Fig. 4 *K* and *L*). In vessels showing both ADan and Aβ deposition, ADan and Aβ were localized to separate areas along the same vessel, with little or no colocalization (Fig. 4*M*).

ADan Accumulation Accelerates Tau Pathology. The occurrence of neurofibrillary Tau pathology in combination with ADan deposition in FDD (4) suggests that ADan and Tau may participate in a common neurodegenerative pathway. To test this experimentally, ADanPP7 mice were crossed to TauP301S tg mice (19). Mice were aged for 12 months, an age at which single TauP301S tg mice have robust Tau lesions in the brainstem and only infrequent lesions in the neocortex (19). Double-tg ADanPP7/TauP301S mice had a >50-fold increase in Gallyas-positive neurofibrillary pathology in the neocortex compared with the single-tg TauP301S littermates (Fig. 5 *A* and *B*). When phosphorylated AT8$^+$ Tau inclusions were counted, an 18-fold increase in neocortex was found in double-tg mice compared with single-tg TauP301S littermates [627.0 ± 277.6 vs. 33.4 ± 13.8; $F(1,11) = 5.396$, $P < 0.04$; n = 6-7/group; all females]. Western blotting of sarcosyl-insoluble Tau confirmed the increase in higher molecular weight insoluble Tau species (64 kDa band) in the forebrain of double-tg mice compared with Tau single-tg siblings (Fig. 5*C*). Immunohistochemistry and Western blotting for ADan did not reveal any changes between double-tg mice and single-tg ADanPP7 littermates (Fig. 5 *D–F*). Finally, predepositing 1.8- to 2-month-old double-tg ADanPP7/TauP301S mice did not reveal any AT8$^+$ Tau inclusions and no difference was noted in AT8-immunoreactivity between the double-tg and single-tg TauP301S mice.

The potentiation of Tau lesions in aged double-tg ADanPP7/TauP301S mice compared with single-tg Tau mice is in all aspects reminiscent of previous studies reporting increased Tau pathology in Tau tg mice crossed with lines that develop Aβ plaque pathology (20–22). To directly compare the ADan-induced Tau lesions to Aβ-induced Tau lesions, APPPS1 mice were crossed with the TauP301S mice and analyzed at 12 months of age. Again, an increase (3- to 4-fold) in AT8$^+$ Tau lesions was observed in the neocortex of double-tg APPPS1/TauP301S mice compared with single-tg TauP301S mice (212 ± 53 vs. 62 ± 50, respectively; n = 8–9/group; males and females combined; P = 0.05). Subsequent comparison of Tau lesions between ADanPP7/TauP301S mice and APPPS1/TauP301S mice by a panel of antibodies against conformationally altered, phosphorylated, and truncated forms of Tau (Table S1) revealed no differences, consistent with the similar morphological and regional appearance of the Tau lesions in the two crosses (Fig. 5*G*).

Discussion

The identification of mutations in BRI2 causing familial British dementia (FBD) and FDD (1, 23) has stimulated intense research into the pathophysiology of these rare diseases. This research interest is sparked because of the similarities between the neuropathological lesions in FBD and FDD and those of AD (4, 12). Modeling FBD and FDD in mice was initially disappointing, but recent work has begun to successfully model FDD in mice (24, 25).

The ADanPP mouse model described here recapitulates the cerebral amyloidosis of FDD. In both ADanPP mice and FDD patients, ADan lesions are abundant in the hippocampus, and also occur in the neocortex (4). The cerebellum in FDD appears to be more affected compared with the mouse model; however, this may be in part a result of the promoter used to drive trangene expression. Most of the ADan lesions in the ADanPP mouse model are associated with the vasculature, as is the case for FDD patients (4). This finding is striking, given that a primarily neuronal promoter was used for the expression of ADanPP. Tg mouse models of cerebral β-amyloidosis using the same PrP promoter accumulate Aβ primarily in the brain parenchyma in form of amyloid plaques (6, 8). These findings argue that properties of the amyloidogenic peptide, in this case Aβ versus ADan, and not the promoter used, can determine in which compartment amyloid formation occurs in the brain (26).

Neuroinflammation is prominent in FDD and in ADanPP mice, with microglia surrounding congophilic ADan deposits and extensive astrocytosis (4). Similarly, dystrophic boutons associated with parenchymal and perivascular amyloid plaques, and amyloid-associated vessel wall degeneration with loss of smooth muscle cells and hemorrhage are seen in both FDD and the ADanPP mouse model (4). All these amyloid-associated changes are remarkably similar to the neurodegeneration, neuroinflammation, and vascular pathology described in AD and in mouse models of cerebral β-amyloidosis (6–9, 14, 26–29). Thus, the shared pathophysiology of ADan and Aβ accumulation suggests that, regardless

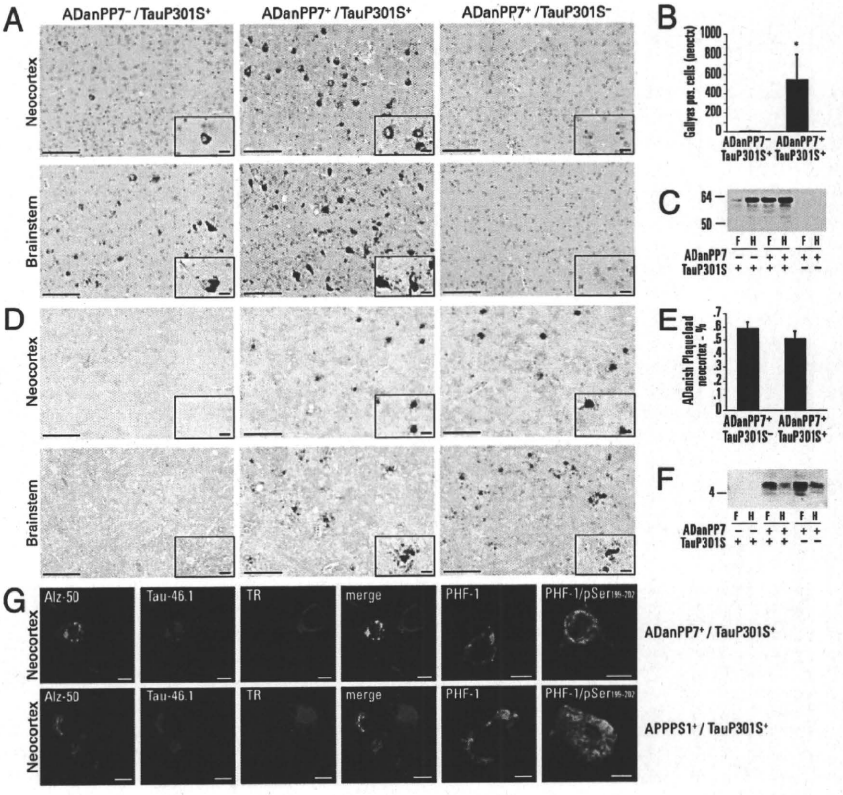

Fig. 5. ADan accelerates the occurrence of Tau lesions in double-tg ADanPP7/TauP301S mice. (*A*) Gallyas silver staining of 12-month-old ADanPP7$^+$/TauP301S$^+$ mice reveals increased Tau lesions in both neocortex and brainstem in comparison with single-tg ADanPP7$^-$/TauP301S$^+$ littermates, with no staining in ADanPP7$^+$/TauP301S$^-$ mice. Inserts are higher magnifications. (*B*) Quantification of neocortical Gallyas-positive cells shows a dramatic increase in ADanPP7$^+$/TauP301S$^+$ mice [all female; n = 6 double tg, n = 7 single tg; $F(1,11) = 5.377$, $P < 0.041$]. (*C*) Western blotting of the sarcosyl insoluble fraction of forebrain "F" and hindbrain "H" homogenates using Ab HT7 reveals an increase in the forebrain of ADanPP7$^+$/TauP301S$^+$ mice (*Lane 3*) in comparison with ADanPP7$^-$/TauP301S$^+$ littermates (*Lane 1*), while the increase in the hindbrain appears smaller (*Lanes 4* and *2*, respectively). (*D* and *E*) No difference in neocortical ADan pathology (Ab 5282) between ADanPP7$^+$/TauP301S$^+$ mice and ADanPP7$^+$/TauP301S$^-$ littermates is observed (*D*) consistent with the stereological quantification [*E*; $F(1,10) = 1.014$, $P = 0.338$; all females; n = 6 double tg, 6 single tg]. (*F*) Western blotting also does not reveal a difference in ADan peptide levels between ADanPP7$^+$/TauP301S$^+$ mice (*Lanes 3* and *4*) in comparison with ADanPP7$^+$/TauP301S$^-$ littermates (*Lanes 5* and *6*). (*G*) Phenotyping of the Tau-lesions in the neocortex of ADanPP7$^+$/TauP301S$^+$ mice reveals a Tau conformation folded at the N terminus (Ab Alz-50) with mostly an intact C terminus (Ab Tau-46.1). The Tau lesions are Thiazin red (TR)-negative, while ADan deposits in the wall of blood vessels are TR-positive (see merger of Alz-50, Tau46.1, and TR staining). The lesions consist of hyperphosphorylated Tau at Ser396-404 (Ab PHF1) and Ser199-202 (Ab pSer199-202). For comparison, phenotyping of the Tau lesions in the neocortex of 12-month-old APPPS1$^+$/TauP301S$^+$ mice reveals the same conformation and phosphorylation pattern. For a list of antibodies and stains, see Table S1. [Scale bars: 100 and 20 μm (*A–F*), 10 μm (*G*).]

of protein sequence, the amyloidogenic properties of the ADan and Aβ peptides are responsible for driving similar downstream disease pathologies.

A common mechanism of amyloid pathophysiology, independent of the sequence of the amyloidogenic peptide, is further supported by our findings that ADan, like Aβ, can induce Tau pathology. Tau lesions in ADanPP mice are absent unless ADanPP mice are crossed with a mouse model overexpressing human mutant Tau. The same is true for APP and APP/PS tg mouse models of AD (20–22). When crossed, the promotion of tau phosphorylation and aggregation appears remarkably similar in ADanPP/TauP301S and in APPPS1/TauP301S mice, and mimics in many aspects human neurofibrillary tangle formation in FDD and AD (4, 30, 31). Thus, our findings suggest that Aβ and ADan (or their respective precursors) share a similar mechanistic link leading to the induction of Tau pathology, possibly mediated by GSK-3 or ChIP (22, 32). The importance of endogenous Tau for Aβ-mediated dysfunction has been recently demonstrated (33), and this may contribute to the behavioral dysfunction of ADanPP mice as well.

However, Aβ and ADan also have distinguishing properties within the brain. The lack of increased amyloid deposition and codeposition in the ADanPP/APP tg mice was unexpected in light of the reported colocalization—and suggested disease-promoting effect—of Aβ and ADan in FDD. However, in patients the colocalization of Aβ and ADan has been reported to be incomplete (4, 12, 13), as was seen in the mice. Our observations of reduced Aβ deposition in the ADanPP/APP tg mice are consistent with previous studies, showing that secreted and potentially amyloidogenic peptides, such as Aβ1–40, Bri2-23, cystatin C, and transthyretin, can inhibit Aβ pathogenesis (34–37). These peptides have been reported to bind Aβ, suggesting that the formation of heterogenous structures may prevent mature amyloid fibril formation (35, 38, 39). Indeed, for cystatin C, the inhibition has been shown to be bidirectional, with Aβ also inhibiting cystatin C dimerization in the brain (35). Understanding the interdependence of Aβ and ADan deposition, however, is complicated by the potential role BRI2 can play in inhibiting APP processing through binding of its transmembrane and Brichos domain to the Aβ region of APP (15–18). Although only a nonsignificant 15 to 17% decrease in Aβ was found in predepositing double-tg ADanPP/APP mice compared with single-tg APP mice, such a steady-state reduction in Aβ generation may be sufficient to account for the observed significant reduction of Aβ deposition several months later. Indeed, that ADan deposition was not affected in the ADanPP/APP crosses is consistent with recent results suggesting that only C-terminal cleaved BRI2 affects APP processing and Aβ generation (18, 40).

A difference between ADanPP mice and mouse models of cerebral β-amyloidosis is the reduced body weight, and (presumed) early death of ADanPP mice (tg mice beyond 24 months of age could not be included in our analyses because mice had to be killed as a result of the significant rate of morbidity). Premature death has only been reported in a few APP and APP/PS1 tg lines and does not appear to be related to the amyloid pathology (6, 33, 41). Although the temporal convergence of ADan deposition and the body-weight loss make a causal link possible, alopecia and kyphosis may indicate that ADanPP expression outside the CNS is responsible for these phenotypes.

Our findings argue that Aβ and ADan, in spite of their lack of sequence homology, participate in similar pathways, leading to neuroinflammation and dementia through their shared amyloid properties. Because ADan does not occur in healthy individuals, our results imply that the relationship between Aβ and AD pathogenesis is likely not directly related to Aβ physiology. Extending our understanding of such shared pathways will lead to the identification of mechanistic

targets for therapeutic intervention common to apparently disparate, albeit pathophysiologically related, neurodegenerative diseases.

Materials and Methods

Generation of ADanPP-Tg Mice. cDNA constructs encoding human BRI2 with the Danish mutation were microinjected into C57BL/6N pronuclei (C57BL/6N-Tg(SHaPrP-BRI2$_{795InsTTTAATTTGT}$). Founders were bred with C57BL/6J mice. For cross-breeding, APPPS1-21 mice (14), APP23 mice (9), and TauP301S mice (19) were used. For details, see *SI Materials and Methods*.

Tissue Preparation, Histology, and Stereology. Formaldehyde-fixed free-floating or paraffin-embedded serial sections were used. For details and antibodies, see *SI Materials and Methods*.

Western Blot and Aβ Immunoassay. For Western blotting, various previously described gel systems were used. Human Aβ40/42 was measured by sandwich immunoassay using MULTI-ARRAY Human (6E10) Aβ ultra-sensitive kits (Meso Scale Discovery). For details see *SI Materials and Methods*.

Behavior Experiments. Morris water-maze testing was done in a circular pool (150 cm diameter). Open-field testing was done in a round open-field (150 cm diameter). All trials were tracked using a Noldus EthoVision system (Noldus Information Technology). Raw data were transferred to the public domain software Wintrack2.4 to calculate the various parameters. For details see *SI Materials and Methods*.

ACKNOWLEDGMENTS. We thank M. Tolnay (Basel) for help with histology; M. Staufenbiel (Basel) for providing APP23 mice; S. Prusiner (San Francisco) and R. Vidal (Indianapolis) for providing the SHaPrP promoter cassette and *BRI2* cDNA; L. Binder (Chicago), P. Davies (Bronx), V. Lee (Philadelphia), M. Novak (Bratislava) for antibodies; and T. Revesz (London) for familial Danish dementia tissue; D. Eicke and N. Rupp for assistance with defining software parameters; and L. Behrends, I. Breuer, C. Krüger, J. Odenthal, and U. Scheurlen (Tübingen) for maintenance of tg lines and veterinary care. This work was supported by a postdoctoral stipend from the Carl-Zeiss Foundation (J.C.); a PhD stipend from the Hertie-Foundation (J.K.H.); the German Research Foundation (JU 655/3-1); the German National Genome Network (NGFNPlus); the Competence Network on Degenerative Dementias (BMBF-01GI0705), Consejo Nacional de Ciencia y Tecnología-Mexico (59651), and the National Center of Competence in Research Neural Plasticity and Repair.

1. Vidal R, et al. (2000) A decamer duplication in the 3' region of the BRI gene originates an amyloid peptide that is associated with dementia in a Danish kindred. *Proc Natl Acad Sci USA* 97:4920–4925.
2. Kim SH, Creemers JW, Chu S, Thinakaran G, Sisodia SS (2002) Proteolytic processing of familial British dementia-associated BRI variants: Evidence for enhanced intracellular accumulation of amyloidogenic peptides. *J Biol Chem* 277:1872–1877.
3. Kim SH, et al. (1999) Furin mediates enhanced production of fibrillogenic ABri peptides in familial British dementia. *Nat Neurosci* 2:984–988.
4. Holton JL, et al. (2002) Familial Danish dementia: A novel form of cerebral amyloidosis associated with deposition of both amyloid-Dan and amyloid-beta. *J Neuropathol Exp Neurol* 61:254–267.
5. Hardy J, Selkoe DJ (2002) The amyloid hypothesis of Alzheimer's disease: Progress and problems on the road to therapeutics. *Science* 297:353–356.
6. Chishti MA, et al. (2001) Early-onset amyloid deposition and cognitive deficits in transgenic mice expressing a double mutant form of amyloid precursor protein 695. *J Biol Chem* 276:21562–21570.
7. Games D, et al. (1995) Alzheimer-type neuropathology in transgenic mice overexpressing V717F beta-amyloid precursor protein. *Nature* 373:523–527.
8. Hsiao K, et al. (1996) Correlative memory deficits, Abeta elevation, and amyloid plaques in transgenic mice. *Science* 274:99–102.
9. Sturchler-Pierrat C, et al. (1997) Two amyloid precursor protein transgenic mouse models with Alzheimer disease-like pathology. *Proc Natl Acad Sci USA* 94: 13287–13292.
10. Small SA, Duff K (2008) Linking Abeta and Tau in late-onset Alzheimer's disease: A dual pathway hypothesis. *Neuron* 60:534–542.
11. Lee HG, et al. (2007) Amyloid-beta in Alzheimer disease: The null versus the alternate hypotheses. *J Pharmacol Exp Ther* 321:823–829.
12. Rostagno A, et al. (2005) Chromosome 13 dementias. *Cell Mol Life Sci* 62:1814–1825.
13. Tomidokoro Y, et al. (2005) Familial Danish dementia: Co-existence of Danish and Alzheimer amyloid subunits (ADan AND Abeta) in the absence of compact plaques. *J Biol Chem* 280:36883–36894.
14. Radde R, et al. (2006) Abeta42-driven cerebral amyloidosis in transgenic mice reveals early and robust pathology. *EMBO Rep* 7:940–946.
15. Fotinopoulou A, et al. (2005) BRI2 interacts with amyloid precursor protein (APP) and regulates amyloid beta (Abeta) production. *J Biol Chem* 280:30768–30772.
16. Matsuda S, et al. (2005) The familial dementia BRI2 gene binds the Alzheimer gene amyloid-beta precursor protein and inhibits amyloid-beta production. *J Biol Chem* 280:28912–28916.
17. Matsuda S, Giliberto L, Matsuda Y, McGowan EM, D'Adamio L (2008) BRI2 inhibits amyloid beta-peptide precursor protein processing by interfering with the docking of secretases to the substrate. *J Neurosci* 28:8668–8676.
18. Peng S, Fitzen M, Jornvall H, Johansson J (2010) The extracellular domain of Bri2 (ITM2B) binds the ABri peptide (1-23) and amyloid beta-peptide (Abeta1-40). Implications for Bri2 effects on processing of amyloid precursor protein and Abeta aggregation. *Biochem Biophys Res Commun* 393:356–361.
19. Allen B, et al. (2002) Abundant Tau filaments and nonapoptotic neurodegeneration in transgenic mice expressing human P301S Tau protein. *J Neurosci* 22:9340–9351.
20. Bolmont T, et al. (2007) Induction of Tau pathology by intracerebral infusion of amyloid-beta -containing brain extract and by amyloid-beta deposition in APP x Tau transgenic mice. *Am J Pathol* 171:2012–2020.
21. Lewis J, et al. (2001) Enhanced neurofibrillary degeneration in transgenic mice expressing mutant Tau and APP. *Science* 293:1487–1491.
22. Terwel D, et al. (2008) Amyloid activates GSK-3beta to aggravate neuronal tauopathy in bigenic mice. *Am J Pathol* 172:786–798.
23. Vidal R, et al. (1999) A stop-codon mutation in the BRI gene associated with familial British dementia. *Nature* 399:776–781.
24. Pickford F, Coomaraswamy J, Jucker M, McGowan E (2006) Modeling familial British dementia in transgenic mice. *Brain Pathol* 16:80–85.
25. Vidal R, Barbeito AG, Miravalle L, Ghetti B (2009) Cerebral amyloid angiopathy and parenchymal amyloid deposition in transgenic mice expressing the Danish mutant form of human BRI2. *Brain Pathol* 19:58–68.
26. Herzig MC, et al. (2004) Abeta is targeted to the vasculature in a mouse model of hereditary cerebral hemorrhage with amyloidosis. *Nat Neurosci* 7:954–960.
27. Adalbert R, et al. (2009) Severely dystrophic axons at amyloid plaques remain continuous and connected to viable cell bodies. *Brain* 132:402–416.
28. Calhoun ME, et al. (1999) Neuronal overexpression of mutant amyloid precursor protein results in prominent deposition of cerebrovascular amyloid. *Proc Natl Acad Sci USA* 96:14088–14093.
29. Stokin GB, et al. (2005) Axonopathy and transport deficits early in the pathogenesis of Alzheimer's disease. *Science* 307:1282–1288.
30. Goedert M, Spillantini MG (2006) A century of Alzheimer's disease. *Science* 314: 777–781.
31. Spires-Jones TL, Stoothoff WH, de Calignon A, Jones PB, Hyman BT (2009) Tau pathophysiology in neurodegeneration: A tangled issue. *Trends Neurosci* 32:150–159.
32. Oddo S, et al. (2008) Blocking Abeta42 accumulation delays the onset and progression of tau pathology via the C terminus of heat shock protein70-interacting protein: A mechanistic link between Abeta and Tau pathology. *J Neurosci* 28:12163–12175.
33. Roberson ED, et al. (2007) Reducing endogenous tau ameliorates amyloid beta-induced deficits in an Alzheimer's disease mouse model. *Science* 316:750–754.
34. Buxbaum JN, et al. (2008) Transthyretin protects Alzheimer's mice from the behavioral and biochemical effects of Abeta toxicity. *Proc Natl Acad Sci USA* 105: 2681–2686.
35. Kaeser SA, et al. (2007) Cystatin C modulates cerebral beta-amyloidosis. *Nat Genet* 39: 1437–1439.
36. Kim J, et al. (2007) Abeta40 inhibits amyloid deposition in vivo. *J Neurosci* 27:627–633.
37. Kim J, et al. (2008) BRI2 (ITM2b) inhibits Abeta deposition in vivo. *J Neurosci* 28: 6030–6036.
38. Mi W, et al. (2007) Cystatin C inhibits amyloid-beta deposition in Alzheimer's disease mouse models. *Nat Genet* 39:1440–1442.
39. Sastre M, et al. (2004) Binding of cystatin C to Alzheimer's amyloid beta inhibits in vitro amyloid fibril formation. *Neurobiol Aging* 25:1033–1043.
40. Matsuda S, Matsuda Y, Snapp EL, D'Adamio L (2009) Maturation of BRI2 generates a specific inhibitor that reduces APP processing at the plasma membrane and in endocytic vesicles. *Neurobiol Aging*, 10.1016/j.neurobiolaging.2009.08.005.
41. Carlson GA, et al. (1997) Genetic modification of the phenotypes produced by amyloid precursor protein overexpression in transgenic mice. *Hum Mol Genet* 6: 1951–1959.
42. Martin L, et al. (2008) Regulated intramembrane proteolysis of Bri2 (Itm2b) by ADAM10 and SPPL2a/SPPL2b. *J Biol Chem* 283:1644–1652.

Journal of the Neurological Sciences 293 (2010) 6–11

Contents lists available at ScienceDirect

Journal of the Neurological Sciences

journal homepage: www.elsevier.com/locate/jns

Occurrence of basophilic inclusions and FUS-immunoreactive neuronal and glial inclusions in a case of familial amyotrophic lateral sclerosis

Zen Kobayashi [a,b,*], Kuniaki Tsuchiya [a,c], Tetsuaki Arai [a], Masashi Aoki [d], Masato Hasegawa [e], Hideki Ishizu [f], Haruhiko Akiyama [a], Hidehiro Mizusawa [b]

[a] Department of Psychogeriatrics, Tokyo Institute of Psychiatry, Tokyo, 156-8585, Japan
[b] Department of Neurology and Neurological Science, Graduate School, Tokyo Medical and Dental University, Tokyo, 113-8519, Japan
[c] Department of Laboratory Medicine and Pathology, Tokyo Metropolitan Matsuzawa Hospital, Tokyo, 156-0057, Japan
[d] Department of Neurology, Tohoku University School of Medicine, Sendai, 980-8574, Japan
[e] Department of Molecular Neurobiology, Tokyo Institute of Psychiatry, Tokyo, 156-8585, Japan
[f] Department of Laboratory Medicine, Zikei Institute of Psychiatry, Okayama, 702-8508, Japan

ARTICLE INFO

Article history:
Received 16 February 2010
Received in revised form 26 March 2010
Accepted 29 March 2010
Available online 20 April 2010

Keywords:
TAR DNA-binding protein of 43 kDa
Frontotemporal lobar degeneration
Immunohistochemistry
Fused in sarcoma
Proteinopathy

ABSTRACT

Basophilic inclusions (BIs) are the pathological feature in a subset of frontotemporal lobar degeneration (FTLD), sporadic amyotrophic lateral sclerosis (SALS) and familial ALS (FALS) cases. Mutations in the *fused in sarcoma (FUS)* gene have been recently identified as the cause of FALS type 6. FUS-immunoreactive (ir) inclusions are consistently found in cases of FTLD with BIs, but the association between ALS cases with BIs and FUS accumulation is still not well understood. In this study, we immunohistochemically analyzed the autopsied case of FALS with BIs using anti-FUS antibodies. The case was a 42-year-old woman who developed proximal weakness of the bilateral upper limbs, followed by weakness of other parts including the bulbar regions, and died at age 45. Since this case is a member of a family with FALS harboring the R521C mutation of the *FUS* gene, she may have carried the same *FUS* mutation. Histopathologically, neuronal loss was evident in the motor system and other areas including the cuneate nucleus of the medulla oblongata. BIs appeared in the brain stem, cerebellum and anterior horn of the lumbar cord. FUS-ir neuronal cytoplasmic inclusions, glial cytoplasmic inclusions and dystrophic neurites were more abundantly and widely occurring than BIs, especially in the cuneate nucleus and globus pallidus. These findings support the idea that both BIs and FUS-ir structures are pathological hallmarks of a subset of ALS cases.

1. Introduction

Amyotrophic lateral sclerosis (ALS) is a neurodegenerative disorder, clinically characterized by upper and lower motor neuron signs, with degenerative changes of the upper and lower motor neurons of the brain and spinal cord [1,2]. Autosomal dominant familial cases account for about 10% of ALS. Thus far, three genes have been confidently linked to familial ALS (FALS): *Cu/Zn superoxide dismutase-1 (SOD1)*, *angiogenin (ANG)*, and the *TAR DNA-binding protein of 43 kDa (TARDBP)*.

Recently, mutations in a gene coding another DNA–RNA binding protein called fused in sarcoma (FUS) have been identified in FALS cases linked to chromosome 16 (ALS6) [3,4]. FUS is a heterogeneous ribonuclear protein (hnRNP) that binds to mRNA/DNA or other hnRNPs through its C-terminus, regulating splicing and transport of pre-mRNA, whereas binding of its N-terminus to polymerases leads to transcriptional activation. A total of 14 different mutations, mostly missenses in exon 15, were reported in the two original studies [3,4]. Neuropathologically, severe lower motor neuron loss in the spinal cord and, to a lesser degree, in the brain stem and mild to moderate upper motor neuron loss in the motor cortex are observed [4]. Immunohistochemical staining of FUS within neuronal and nonneuronal nuclei is observed in both control and patient sections [3], while additional prominent cytoplasmic FUS staining [3] or elongated inclusions in spinal cord motor neurons and dystrophic neurites (DNs) [4] are found only in patient sections.

Subsequent studies have found FUS-immunoreactive (ir) neuronal cytoplasmic inclusions (NCIs) and glial cytoplasmic inclusions (GCIs) in tau-negative and TDP-43-negative frontotemporal lobar degeneration (FTLD), including atypical FTLD with ubiquitinated inclusions (aFTLD-U) [5], in neuronal intermediate filament inclusion disease (NIFID) [6], and in basophilic inclusion body disease (BIBD) [7].

Basophilic inclusions (BIs) were first described in sporadic ALS (SALS) showing onset in the teens [8–12], and then have been reported in SALS with onset in the twenties [13–15], thirties [16–18],

* Corresponding author. Department of Psychogeriatrics, Tokyo Institute of Psychiatry, Tokyo Metropolitan Organization for Medical Research, 2-1-8 Kamikitazawa, Setagaya-ku, Tokyo, 156-8585, Japan.
E-mail address: zen@bg7.so-net.ne.jp (Z. Kobayashi).

0022-510X/$ – see front matter © 2010 Elsevier B.V. All rights reserved.
doi:10.1016/j.jns.2010.03.029

forties [19], fifties [20,21] and sixties [22]. Munoz et al. reported the occurrence of FUS-ir NCIs, DNs and GCIs in the two cases of SALS with BIs, which were previously reported by Kusaka et al. [7,17,20]. More recently, Tateishi et al. have identified the R521C mutation of *FUS* in FALS cases with BIs, and found FUS-ir BIs and GCIs in affected lesions [23]. Suzuki et al. have also reported another Japanese FALS family with the R521C *FUS* mutation and BIs [24]. These findings suggest the possibility that occurrences of both BIs and FUS-ir structures are pathological hallmarks of a subset of FALS and SALS cases. To further validate this hypothesis, in this study, we immunohistochemically reevaluated a previously reported case of FALS with BIs [25], using anti-FUS antibodies. This case is a member of the family with FALS reported by Suzuki et al. [24], suggesting that she may carry the R521C *FUS* mutation.

2. Case report

A 42-year-old Japanese woman developed muscle weakness of the proximal part of the bilateral upper limbs. There were 23 patients with ALS over four generations in her family (Fig. 1), in a member of which the R521C mutation of the *FUS* gene has been identified [24]. Neurological examination at age 43 showed dysarthria, muscle weakness and atrophy in the bilateral upper limbs with proximal dominance, spasticity in the right upper limb and bilateral lower limbs, and hyperreflexia in the bilateral lower limbs. At the same age, she presented with dysphasia. At age 44, she developed difficulty in respiration, and neurological examination showed muscle weakness and atrophy in the four limbs with upper limb dominance and a bilateral Babinski's sign. At the same age, she required artificial respiratory support, and died of bronchopneumonia about one year and five months later. The total disease duration was three years and one month. There was no sensory disturbance, ataxia or parkinsonism in the clinical course. No dementia or behavioral abnormalities were detected as well.

3. Methods

3.1. Neuropathological examination

Brain tissue samples were fixed postmortem with 10% formalin and embedded in paraffin. Ten-μm thick sections were prepared from the frontal, temporal, parietal, occipital, insular, and cingulate cortices, hippocampus, amygdala, basal ganglia, midbrain, pons, medulla oblongata, cerebellum and spinal cord including the cervical, thoracic, lumbar and sacral cord. These sections were stained by the hematoxylin–eosin (HE) and Klüver–Barrera (KB) methods. The severity of neuronal loss and tract degeneration was evaluated as none (−), mild (+) or severe (++); Table 1.

3.2. Immunohistochemistry

Most immunohistochemistry was performed using the Ventana Discovery XT automated staining system (Roche, Tokyo, Japan) and developed with diaminobenzidine (DAB). Antibodies employed in this study are shown in Table 2. FUS-ir structures were assessed according to the grading system of the previous studies [6], and are indicated as none (0), rare (1+), occasional (2+), common (3+) or numerous (4+) in Table 1. Immunoreactivity (IR) of cystatin C, ubiquitin and TDP-43 was examined in the brainstem and spinal cord.

4. Results

4.1. Macroscopic findings

Brain weight was 1100 g. There were no abnormalities in the brain on macroscopic examination. The anterior roots of the spinal cord were atrophic, and the anterior horn of the cervical cord was also atrophic.

4.2. Microscopic findings

Marked neuronal loss was observed in the anterior horn of the spinal cord (Fig. 2A–C), cuneate nucleus (Fig. 2D, E) and hypoglossal nucleus (Fig. 2F). Neuronal loss was also seen in Clarke's column, the gracile nucleus, motor nucleus of the trigeminal nerve, substantia nigra, and globus pallidus in milder degree. In the primary motor cortex, Betz cells were sparse in comparison with normal controls. In the cervical cord, the lateral part of the anterior horn was markedly atrophic (Fig. 2A). In the whole spinal cord, the anterior and lateral funiculi including the spinothalamic and spinocerebellar tracts were extensively degenerated, while the anterior and lateral corticospinal tract (CST) was relatively spared (Fig. 2A). In the posterior funiculus of the upper thoracic and cervical cord, degeneration was evident in the cuneate fasciculus, whereas the gracile fasciculus was less affected (Fig. 2A). In the lumbar cord, degeneration was demonstrated in the posterior funiculus corresponding to the gracile fasciculus (Fig. 2B). There was slight gliosis in the pontine base and subthalamic nucleus, but neuronal loss was not apparent in these regions. Ischemic changes and a mild loss of Purkinje cells were seen.

The BIs were best seen in KB-stained sections, and were demonstrated in the Betz cells (Fig. 2G), subthalamic nucleus, substantia nigra, periaqueductal gray matter, locus ceruleus, pontine nucleus (Fig. 2H), lateral cuneate nucleus (Fig. 2I), gracile nucleus, reticular formation of the medulla oblongata, cerebellar dentate nucleus and anterior horn of the lumbar cord (Fig. 2J). Most BIs were homogenous and round with no halo or core as previously reported [17,20]. The color of the BIs in HE-stained sections was near to pink (Fig. 2I, J), rather than blue, with occasional thin basophilic rim

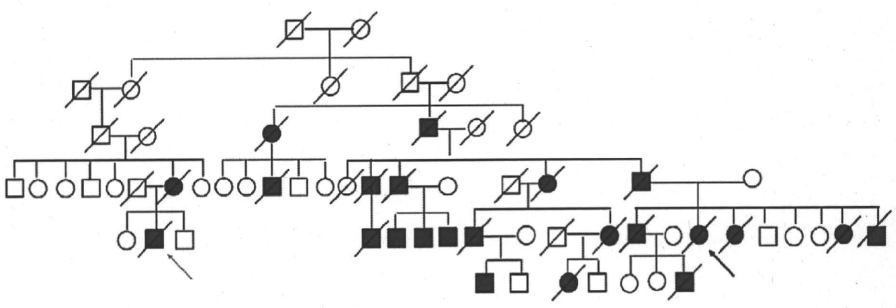

Fig. 1. Pedigree of a Japanese family with FALS harboring a *FUS* mutation. Males are represented by square, females by circles. Affected members are represented by solid symbols, deceased individuals by diagonals. The gray and black arrows indicate the proband harboring the R521C *FUS* mutation and the present case, respectively.

Table 1
Distribution and severity of lesions across scanned central nervous system regions.

	DEG	BI	NCI	DN	GCI
Cerebrum					
Corpus callosum	−	N	N	N	−
Cingulate gyrus cortex	−	−	−	−	−
Cingulate white matter	−	N	N	N	−
Frontal cortex	−	−	1	−	1
Frontal white matter	−	N	N	N	−
Primary motor cortex	−	p	1	−	1
Primary motor white matter	−	N	N	N	1
Amygdala	−	−	−	−	−
Hippocampal dentate gyrus	−	−	−	−	−
Hippocampal CA	−	−	−	−	−
Subiculum	−	−	−	−	−
Temporal cortex	−	−	−	−	−
Temporal white matter	−	N	N	N	−
Caudate nucleus	−	−	−	−	−
Putamen	−	−	1	−	2
Globus pallidus	+	−	3	2	4
Thalamus	−	−	1	−	1
Subthalamic nucleus	−	p	N	N	N
Meynert nucleus	−	−	−	−	1
Midbrain					
Substantia nigra	+	p	2	1	3
Periaqueductal gray matter	−	p	3	1	1
Oculomotor nucleus	−	−	1	−	1
Trochlear nucleus	−	−	N	N	N
Reticular formation	N	−	1	1	2
Red nucleus	−	−	−	1	−
Medial longitudinal fasciculus	−	N	N	N	N
Cerebral peduncle	−	N	N	N	1
Pons					
Motor nucleus of trigeminal nerve	+	−	N	N	N
Locus ceruleus	−	p	1	−	−
Reticular formation	N	N	2	2	1
Central tegmental tract	−	N	N	N	1
Superior cerebellar peduncle	−	N	N	N	−
Pontine nucleus	−	p	1	−	−
Pyramidal tract	−	N	N	N	1
Medulla oblongata					
Hypoglossal nucleus	++	−	−	1	1
Dorsal vagal nucleus	−	−	1	−	−
Nucleus tractus soritarius	−	−	−	−	−
Gracile nucleus	+	p	N	N	N
Cunetate nucleus	++	p	4	1	1
Spinal nucleus of trigeminal nerve	N	−	1	1	1
Inferior olivary nucleus	−	−	−	−	1
Reticular formation	N	p	3	2	3
Medial lemniscus	−	N	N	N	1
Pyramid	−	N	N	N	1
Cerebellum					
Purkinje cells	+	−	−	−	−
Dentate nucleus	−	p	2	−	−
White matter	−	N	N	N	−
Spinal cord					
Anterior horn	++	p	2	1	3
Posterior horn	N	−	1	N	1
Clarke's nucleus	+	−	−	−	−
Intermediolateral horn	−	−	−	−	−
Anterior and lateral CST	+	N	N	N	1
Anterior and lateral funiculi[a]	++	N	N	N	2
Cuneate fasciculus	++	N	N	N	1
Gracile fasciculus	+	N	N	N	−

DEG: degeneration assessed on the HE- and KB-stained sections. The degeneration was indicated as none (−), mild (+) or severe (++). *BI:* basophilic inclusion. The BIs were indicated as absent (−) or present (p). *NCI:* FUS-immunoreactive (ir) neuronal cytoplasmic inclusion, *GCI:* FUS-ir glial cytoplasmic inclusion. *DN:* FUS-ir dystrophic neuritis, *N:* not evaluated (or not able to evaluate) The FUS pathology was indicated as none (−), rare (1), occasional (2), common (3) or numerous (4). *CST:* corticospinal tract.
[a] This means the region outside the CST.

(Fig. 2J), which is consistent with some previous descriptions [7,17,18,20]. Neuronal cytoplasmic vacuolar changes similar to granulovacuolar degeneration were sometimes observed (Fig. 2I).

Table 2
Antibodies used in immunohistochemistry.

Antibody	Type	Source	Dilution
Anti-ubiquitin	Rabbit polyclonal	Dako, Glostrup, Denmark	1:500
Anti-p62	Rabbit polyclonal	Biomol, Philadelphia, USA	1:1000
Anti-phosphorylated TDP-43 (pS409/410)	Rabbit serum	Made by Hasegawa et al. [36]	1:1000
Anti-FUS	Rabbit polyclonal	Sigma, St. Louis, MO, USA	1:200
Anti-FUS	Rabbit polyclonal	Made by Doi et al. [37]	1:500
Anti-cystatin C	Rabbit polyclonal	Dako, Glostrup, Denmark	1:3000

4.3. Immunohistochemical findings

FUS immunohistochemistry showed a widespread distribution of NCIs (Fig. 3A–F), GCIs (Fig. 3D) and DNs (Fig. 3G) in the cerebrospinal regions. Most NCIs were round (Fig. 3A–D), but crescentic (Fig. 3E) or mushroom-shaped (Fig. 3F) NCIs were also found. Round or irregular-shaped FUS-ir structures of similar size to the NCIs but lacking an outline of the neuron were sometimes observed within the neuropil in the globus pallidus, cuneate nucleus and anterior horn of the spinal cord (Fig. 3H). There was no or very weak FUS IR in the nucleus and the cytoplasm of neurons and glial cells without inclusions in all cerebrospinal regions examined. Neuronal intranuclear inclusions (NIIs) were absent.

The number of FUS-ir NCIs was greater than that of the BIs which were visible with KB or HE stain. In general, NCIs were preferentially observed in large neurons, and were hardly seen in small neurons. FUS-ir structures were numerous in the cuneate nucleus and globus pallidus. Other areas containing FUS-ir structures were the pyramidal cell layer of the frontal cortex, including the primary motor cortex, putamen, thalamus, substantia nigra, periaqueductal gray matter, oculomotor nucleus, locus ceruleus, pontine nucleus, hypoglossal nucleus, dorsal vagal nucleus, spinal nucleus of the trigeminal nerve, reticular formation of the brainstem, cerebellar dentate nucleus, and anterior and posterior horns of the spinal cord. There were no obvious differences in the distribution of NCIs, GCIs and DNs. The distribution and degree of degeneration and FUS-ir structures are summarized in Table 1. p62 immunohistochemistry also labeled some NCIs, but ubiquitin immunohistochemistry did not label any NCIs. No Bunina bodies were identified even by cystatin C immunohistochemistry.

5. Discussion

This is the second report of an autopsied FALS case with BIs showing a widespread occurrence of FUS-ir neuronal and glial inclusions. Unfortunately, the sequence analysis of *FUS* gene in this case could not be performed because only formalin-fixed and paraffin-embedded tissues were available. However, Suzuki et al. recently identified the R521C *FUS* mutation in an ALS patient [24], who is a member of the family of the present case, suggesting that she may have carried the same *FUS* mutation.

FUS mutations have been found in 3–5% of patients with FALS [3,4,26–29], and in some SALS cases [28,30,31]. The R521C mutation is one of the most common mutations [3], and the mean age at onset and disease duration of the cases with this mutation were 42.9 years and 1.9 years, respectively [26]. Among cases with this mutation, weakness of the neck and/or proximal upper limbs is frequently seen [23,26,29], and bulbar dysfunction, dystonia or frontotemporal dementia is rarely observed [26]. There is no sensory disturbance, ataxia or parkinsonism. The clinical features of the present case are largely consistent with those previously reported.

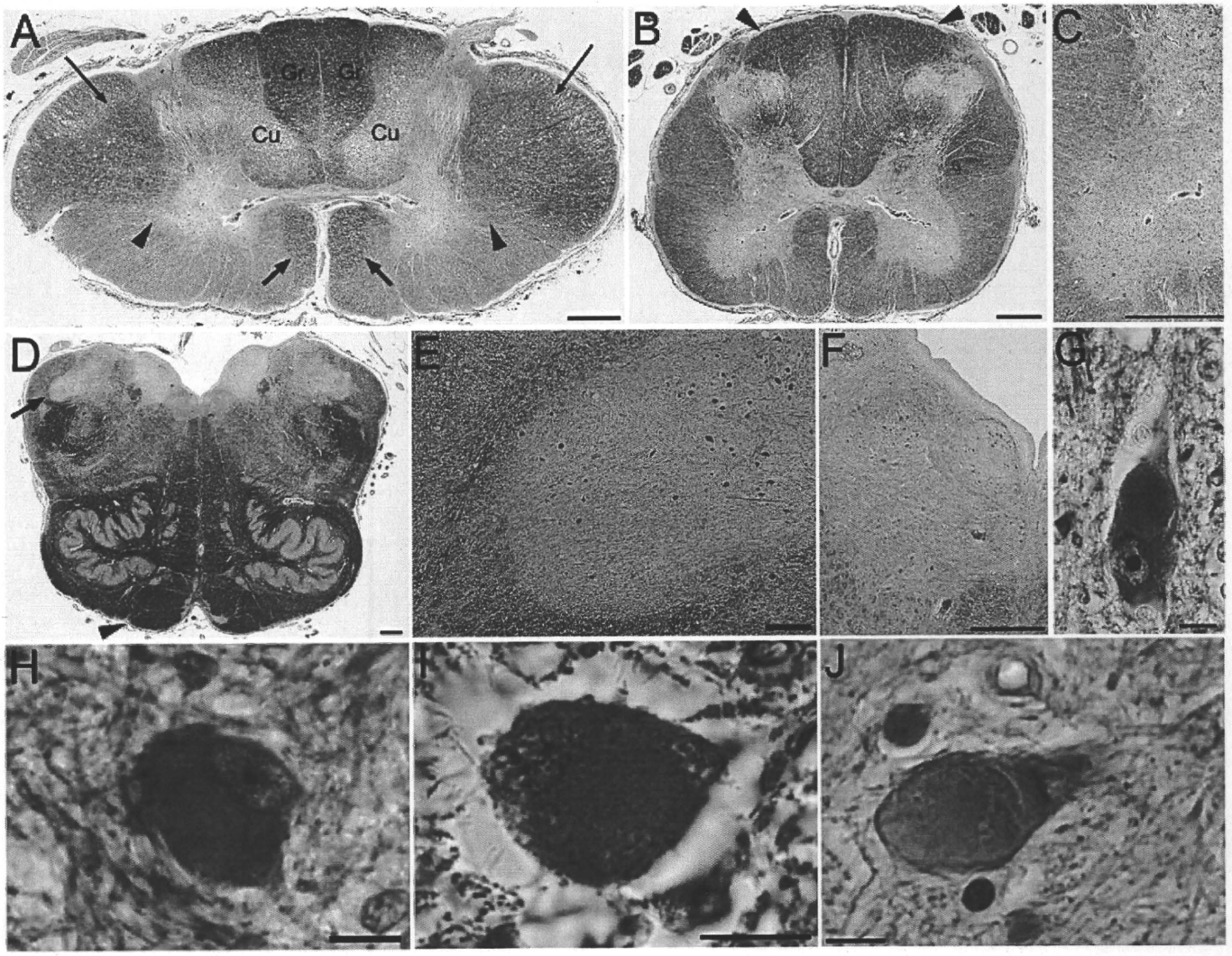

Fig. 2. A. The lateral part of the anterior horn is atrophic in the cervical segment 6 (arrowheads). The anterior and lateral funiculi are extensively degenerated while the anterior (short arrows) and lateral (long arrows) corticospinal tract is less affected. In the posterior funiculus, degeneration is evident in the cuneate fasciculus (indicated by Cu), whereas the gracile fasciculus is relatively preserved (indicated by Gr). B. In the lumbar segment 3, extensive white matter degeneration is demonstrated in the anterior and lateral funiculi, and posterior funiculus corresponding to the gracile fasciculus. Only the periphery of the posterior funiculus was preserved (arrowheads). C. A high power view of the right anterior horn shows almost complete neuronal loss. D. The medulla oblongata at the level of caudal end of the fourth ventricle is shown. The CST degeneration is not apparent at the pyramid (arrowhead). The arrow indicates the right lateral cuneate nucleus. E. A high power view of the right lateral cuneate nucleus demonstrates evident loss of neurons and myelin. F. The right hypoglossal nucleus shows complete neuronal loss. G. The neuronal cytoplasmic inclusion (NCI) in the Betz cell is larger than the nucleus, and show intense and homogenous staining without halo or core. H. In a neuron of the pontine nucleus, the NCI is recognized by the presence of the outline, and the nucleus is located in the periphery. I. The basophilia is not apparent in the NCI in the cuneate nucleus. Neuronal cytoplasmic vacuolar changes similar to granulovacuolar degeneration are observed. J. The NCI showing a thin basophilic rim in the intermediate zone of the anterior horn of the lumbar segment 4. A–H. Klüver–Barrera stain, I, J. hematoxylin–eosin stain. Scale bar A–D. 1 mm, E. 200 μm, F. 500 μm, G–J. 10 μm.

To date, four papers have described the neuropathology of the patients with the R521C mutation [3,4,23,26], but details were reported only by Tateishi et al. [23]. Our case is neuropathologically characterized by severe neuronal loss in the cuneate nucleus and extensive white matter degeneration of the spinal cord with relative preservation of the CST. It is noteworthy that the distributions of FUS-ir structures and that of degeneration were largely parallel in the cerebrospinal regions (Table 1). These findings suggest that FUS accumulation plays an important role in the degeneration. In the first autopsied FALS case with BIs and FUS-ir structures, reported by Tateishi et al. [23], degenerative changes and FUS-ir structures were more severe and widely distributed throughout the cerebrospinal regions, including the frontotemporal cortex, hippocampus, thalamus, and brain stem, than in our case. One reason for such a discrepancy may be the longer disease duration of their case than of ours. It has already been reported that a widespread and severe degeneration is frequently seen in ALS cases showing long-term survival with artificial respiratory support [21,32,33].

The normal physiological staining pattern of FUS has been reported to consist of strong IR of neuronal nuclei, weaker but consistent staining of neuronal cytoplasm and more variable IR of glial nuclei in normal controls, aFTLD-U [5], NIFID [6], and BIBD [7]. In both the nuclei and cytoplasm, the normal staining pattern is generally diffuse but with occasional small granules [5]. Neumann et al. reported that in cells with FUS-ir inclusions in aFTLD-U and NIFID, at least some of such normal nuclear and cytoplasmic distribution of FUS staining is retained [5,6]. Munoz et al. indicated that in BIBD, the presence of FUS-ir NCI was accompanied by total or partial loss of nuclear FUS IR in some cells, whereas others maintained a normal level of nuclear staining [7]. This variability of FUS IR is in contrast to the consistent reduction in nuclear TDP-43 staining in cells harboring TDP-43-ir inclusions [34]. In the case with the R521C mutation

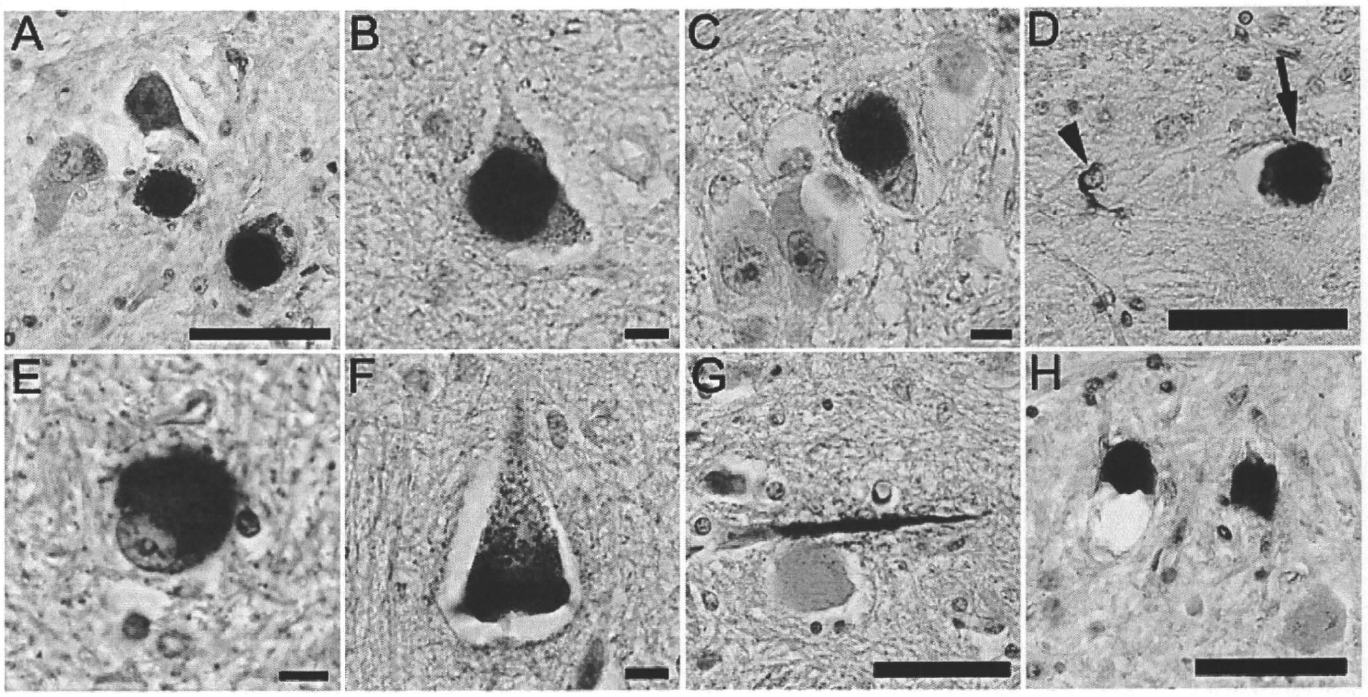

Fig. 3. Anti-FUS antibodies show round NCIs in the cuneate nucleus (A), periaqueductal gray matter (B), pontine nucleus (C) and globus pallidus (D, arrow), and a GCI in the globus pallidus (D, arrowhead). Crescentic (E) or mushroom-shaped (F) NCIs are also found. A long DN is seen in the spinal nucleus of the trigeminal nerve (G). In the neuropil of the cuneate nucleus, there are round or irregular-shaped FUS-immunoreactive structures showing similar size to the NCIs but lacking outline of the neuron (H). Scale bar A, D, G, H. 50 μm, B, C, E, F. 10 μm.

reported by Tateishi et al. [23], on the other hand, faint diffuse nuclear immunostaining to FUS with prominent nucleolar staining was seen in neurons without inclusions, while such nuclear FUS IR was lost in neurons bearing inclusions [23]. Thus, there is some discrepancy in FUS IR between reports or diseases. Furthermore, the absence or very weak FUS IR in the nucleus and cytoplasm of neurons and glial cells without inclusions in our case differs from these previous findings. The most plausible explanation for that may be due to the high fixation-related variation in IR for anti-FUS antibodies as previously reported [7]. In immunohistochemistry, FUS proteins physiologically distributed in the nucleus and cytoplasm may be more vulnerable to the influence of fixation than those abnormally accumulated. This should be further examined by more detailed histochemical studies using a larger number of FALS cases with BIs.

Rounded FUS-ir structures of similar size to the NCIs but lacking an outline of the cell body and nucleus were found in our case (Fig. 2H) but have not so far been described in cases of aFTLD-U, NIFID, BIBD and FALS with *FUS* mutations. They may represent a residual form of inclusions after neuronal death, similar to the ghost tangles in Alzheimer's disease or the extracellular Lewy bodies in dementia with Lewy bodies [35]. It could be important to clarify whether they are specific for a subset of FALS with BI cases or whether they are commonly found in other disorders with FUS accumulation.

It is known that there are many similarities between FUS and TDP-43. They are DNA/RNA binding proteins involved in transcriptional regulation, mRNA splicing, transport and translation [5]. Mutations in both genes cause ALS, and both gene products accumulate in neurons and glial cells. Clinically, both cases with FUS pathology and those with TDP-43 pathology can present as ALS, FTLD, or a combination of the two [7]. However, there are some differences between the two proteins, including their intracellular localization in the normal physiological state and the degree of their nuclear localization in cells harboring inclusions, as mentioned above. In terms of the morphology of NCIs in the spinal cord, skein-like inclusions are one of the pathological hallmarks of TDP-43-associated ALS, while more rounded NCIs are the major species in FUS-related ALS. Furthermore, the abundant occurrence of NCIs which we found in the cuneate nucleus and globus pallidus has not so far been reported in TDP-43-associated ALS cases. Thus, regardless of their functional similarities, FUS and TDP-43 may contribute to the development of ALS and FTLD by distinct molecular pathways. The normal roles of both proteins in brains and the pathological effect of mutations of the genes encoding them should be further investigated to elucidate the pathogenesis of these disorders.

In conclusion, we demonstrated a widespread occurrence of FUS-ir neuronal and glial structures in a case of FALS with BIs in this study. Further studies using a larger number of cases are needed to prove the hypothesis that the cases of FALS and SALS with BIs share a common pathological process associated with the FUS abnormality.

Acknowledgements

This work was supported by Grants-in-Aid from the Ministry of Health, Labour and Welfare of Japan, Grants-in-Aid for scientific research from the Ministry of Education, Culture, Sports, Science and Technology (14570957) and a research grant from the Zikei Institute of Psychiatry. The authors thank Yo Shoda and Kyoko Suzuki (Tokyo Institute of Psychiatry) for the excellent photographic assistance, and Ms Hiromi Kondo and Chie Haga (Tokyo Institute of Psychiatry) for the excellent technical assistance.

References

[1] Ravits JM, La Spada AR. ALS motor phenotype heterogeneity, focality, and spread: deconstructing motor neuron degeneration. Neurology 2009;73:805–11.
[2] Tsuchiya K, Ikeda K, Mimura M, Takahashi M, Miyazaki H, Anno M, et al. Constant involvement of the Betz cells and pyramidal tract in amyotrophic lateral sclerosis with dementia: a clinicopathological study of eight autopsy cases. Acta Neuropathol 2002;104:249–59.
[3] Kwiatkowski Jr TJ, Bosco DA, Leclerc AL, Tamrazian E, Vanderburg CR, Russ C, et al. Mutations in the FUS/TLS gene on chromosome 16 cause familial amyotrophic lateral sclerosis. Science 2009;323:1205–8.
[4] Vance C, Rogelj B, Hortobágyi T, De Vos KJ, Nishimura AL, Sreedharan J, et al. Mutations in FUS, an RNA processing protein, cause familial amyotrophic lateral sclerosis type 6. Science 2009;323:1208–11.

[5] Neumann M, Rademakers R, Roeber S, Baker M, Kretzschmar HA, Mackenzie IR. A new subtype of frontotemporal lobar degeneration with FUS pathology. Brain 2009;132:2922–31.
[6] Neumann M, Roeber S, Kretzschmar HA, Rademakers R, Baker M, Mackenzie IR. Abundant FUS-immunoreactive pathology in neuronal intermediate filament inclusion disease. Acta Neuropathol 2009;118:605–16.
[7] Munoz DG, Neumann M, Kusaka H, Yokota O, Ishihara K, Terada S, et al. FUS pathology in basophilic inclusion body disease. Acta Neuropathol 2009;118:617–27.
[8] Berry RG, Chambers RA, Duckett S, Terraro R. Clinicopathological study of juvenile amyotrophic lateral sclerosis. Neurology 1969;19:312.
[9] Nelson JS, Prensky AL. Sporadic juvenile amyotrophic lateral sclerosis. A clinicopathological study of a case with neuronal cytoplasmic inclusions containing RNA. Arch Neurol 1972;27:300–6.
[10] Oda M, Akagawa N, Tabuchi Y, Tanabe H. A sporadic juvenile case of the amyotrophic lateral sclerosis with neuronal intracytoplasmic inclusions. Acta Neuropathol 1978;44:211–6.
[11] Tsujihata M, Taguchi H, Oku Y, Takamori M, Terao H. A sporadic case of juvenile amyotrophic lateral sclerosis. Rinsho Shinkeigaku 1978;18:82–8.
[12] Wohlfarte G, Swank RL. Pathology of amyotrophic lateral sclerosis. Arch Neurol Psychiatry 1941;46:783–99.
[13] Aizawa H, Kimura T, Hashimoto K, Yahara O, Okamoto K, Kikuchi K. Basophilic cytoplasmic inclusions in a case of sporadic juvenile amyotrophic lateral sclerosis. J Neurol Sci 2000;176:109–13.
[14] Hilton DA, McLean B. December 2001: rapidly progressive motor weakness, starting in pregnancy. Brain Pathol 2002;12:267–8.
[15] Matsumoto S, Kusaka H, Murakami N, Hashizume Y, Okazaki H, Hirano A. Basophilic inclusions in sporadic juvenile amyotrophic lateral sclerosis: an immunocytochemical and ultrastructural study. Acta Neuropathol 1992;83:579–83.
[16] Hamada K, Fukazawa T, Yanagihara T, Yoshida K, Hamada T, Yoshimura N, et al. Dementia with ALS features and diffuse Pick body-like inclusions (atypical Pick's disease?). Clin Neuropathol 1995;14:1–6.
[17] Kusaka H, Matsumoto S, Imai T. An adult-onset case of sporadic motor neuron disease with basophilic inclusions. Acta Neuropathol 1990;80:660–5.
[18] Yokota O, Tsuchiya K, Terada S, Ishizu H, Uchikado H, Ikeda M, et al. Basophilic inclusion body disease and neuronal intermediate filament inclusion disease: a comparative clinicopathological study. Acta Neuropathol 2008;115:561–75.
[19] Sam M, Gutmann L, Schochet Jr SS, Doshi H. Pick's disease: a case clinically resembling amyotrophic lateral sclerosis. Neurology 1991;41:1831–3.
[20] Kusaka H, Matsumoto S, Imai T. Adult-onset motor neuron disease with basophilic intraneuronal inclusion bodies. Clin Neuropathol 1993;12:215–8.
[21] Mizutani T, Sakamaki S, Tsuchiya N, Kamei S, Kohzu H, Horiuchi R, et al. Amyotrophic lateral sclerosis with ophthalmoplegia and multisystem degeneration in patients on long-term use of respirators. Acta Neuropathol 1992;84:372–7.
[22] Sasaki S, Toi S, Shirata A, Yamane K, Sakuma H, Iwata M. Immunohistochemical and ultrastructural study of basophilic inclusions in adult-onset motor neuron disease. Acta Neuropathol 2001;102:200–6.
[23] Tateishi T, Hokonohara T, Yamasaki R, Miura S, Kikuchi H, Iwaki A, et al. Multiple system degeneration with basophilic inclusions in Japanese ALS patients with FUS mutation. Acta Neuropathol 2010;119:355–64.
[24] Suzuki N, Aoki M, Warita H, Kato M, Mizuno H, Shimakura N, et al. FALS with FUS mutation in Japan with early onset, rapid progress and basophilic inclusion. J Hum Genet 2010 doi:10.1038/jhg.2010.16.
[25] Tsuchiya K, Matsunaga T, Aoki M, Haga C, Ooe K, Abe K, et al. Familial amyotrophic lateral sclerosis with posterior column degeneration and basophilic inclusion bodies: a clinical, genetic and pathological study. Clin Neuropathol 2001;20:53–9.
[26] Blair IP, Williams KL, Warraich ST, Durnall JC, Thoeng AD, Manavis J, et al. FUS mutations in amyotrophic lateral sclerosis: clinical, pathological, neurophysiological and genetic analysis. J Neurol Neurosurg Psychiatry 2010 doi:10.1136/jnnp.2009.194399.
[27] Chiò A, Restagno G, Brunetti M, Ossola I, Calvo A, Mora G, et al. Two Italian kindreds with familial amyotrophic lateral sclerosis due to FUS mutation. Neurobiol Aging 2009;30:1272–5.
[28] Corrado L, Del Bo R, Castellotti B, Ratti A, Cereda C, Penco S, et al. Mutations of FUS gene in sporadic amyotrophic lateral sclerosis. J Med Genet 2010 doi: 10.1136/jmg.2009.071027.
[29] Ticozzi N, Silani V, LeClerc AL, Keagle P, Gellera C, Ratti A, et al. Analysis of FUS gene mutation in familial amyotrophic lateral sclerosis within an Italian cohort. Neurology 2009;73:1180–5.
[30] Belzil VV, Valdmanis PN, Dion PA, Daoud H, Kabashi E, Noreau A, et al. Mutations in FUS cause FALS and SALS in French and French Canadian populations. Neurology 2009;73:1176–9.
[31] Drepper C, Herrmann T, Wessig C, Beck M, Sendtner M. C-terminal FUS/TLS mutations in familial and sporadic ALS in Germany. Neurobiol Aging 2010 doi: 10.1016/j.neurobiolaging.2009.11.017.
[32] Kato S, Hayashi H, Oda M, Kawata A, Shimizu T, Hayashi M, et al. Neuropathology in sporadic ALS patients on respirators. In: Nakano I, Hirano A., eds. Amyotrophic lateral sclerosis: progress and perspectives in basic research and clinical application. Amsterdam: Elsevier. pp. 66–77.
[33] Nishihira Y, Tan CF, Onodera O, Toyoshima Y, Yamada M, Morita T, et al. Sporadic amyotrophic lateral sclerosis: two pathological patterns shown by analysis of distribution of TDP-43-immunoreactive neuronal and glial cytoplasmic inclusions. Acta Neuropathol 2008;16:169–82.
[34] Neumann M, Sampathu DM, Kwong LK, Truax AC, Micsenyi MC, Chou TT, et al. Ubiquitinated TDP-43 in frontotemporal lobar degeneration and amyotrophic lateral sclerosis. Science 2006;314:130–3.
[35] Iseki E, Marui W, Akiyama H, Uéda K, Kosaka K. Degeneration process of Lewy bodies in the brains of patients with dementia with Lewy bodies using alpha-synuclein-immunohistochemistry. Neurosci Lett 2000;286:69–73.
[36] Hasegawa M, Arai T, Nonaka T, Kametani F, Yoshida M, Hashizume Y, et al. Phosphorylated TDP-43 in frontotemporal lobar degeneration and amyotrophic lateral sclerosis. Ann Neurol 2008;64:60–70.
[37] Doi H, Okamura K, Bauer PO, Furukawa Y, Shimizu H, Kurosawa M, et al. RNA-binding protein TLS is a major nuclear aggregate-interacting protein in huntingtin exon 1 with expanded polyglutamine-expressing cells. J Biol Chem 2008;283:6489–500.